Published December 8, 2016

Fine-tuning of ULK1 mRNA and protein levels is required for autophagy oscillation

Francesca Nazio,[1,2] Marianna Carinci,[2] Cristina Valacca,[2] Pamela Bielli,[3] Flavie Strappazzon,[3] Manuela Antonioli,[4,5] Fabiola Ciccosanti,[5] Carlo Rodolfo,[2] Silvia Campello,[2,3] Gian Maria Fimia,[5,6] Claudio Sette,[3,7] Paolo Bonaldo,[8] and Francesco Cecconi[1,2,9]

[1]Department of Pediatric Hematology and Oncology, Istituto di Ricovero e Cura a Carattere Scientifico Bambino Gesù Children's Hospital, 00146 Rome, Italy
[2]Department of Biology, University of Rome Tor Vergata, 00133 Rome, Italy
[3]Istituto di Ricovero e Cura a Carattere Scientifico Fondazione Santa Lucia, 00143 Rome, Italy
[4]Freiburg Institute for Advanced Studies, University of Freiburg, 79104 Freiburg, Germany
[5]National Institute for Infectious Diseases, Istituto di Ricovero e Cura a Carattere Scientifico "L. Spallanzani," 00149 Rome, Italy
[6]Department of Biological and Environmental Sciences and Technologies, University of Salento, 73100 Lecce, Italy
[7]Department of Biomedicine and Prevention, University of Rome Tor Vergata, 00133 Rome, Italy
[8]Department of Molecular Medicine, University of Padova, 35131 Padova, Italy
[9]Danish Cancer Society Research Center, 2100 Copenhagen, Denmark

Autophagy is an intracellular degradation pathway whose levels are tightly controlled to secure cell homeostasis. Unc-51–like kinase 1 (ULK1) is a conserved serine–threonine kinase that plays a central role in the initiation of autophagy. Here, we report that upon autophagy progression, ULK1 protein levels are specifically down-regulated by the E3 ligase NEDD4L, which ubiquitylates ULK1 for degradation by the proteasome. However, whereas ULK1 protein is degraded, *ULK1* mRNA is actively transcribed. Upon reactivation of mTOR-dependent protein synthesis, basal levels of ULK1 are promptly restored, but the activity of newly synthesized ULK1 is inhibited by mTOR. This prepares the cell for a new possible round of autophagy stimulation. Our results thus place NEDD4L and ULK1 in a key position to control oscillatory activation of autophagy during prolonged stress to keep the levels of this process under a safe and physiological threshold.

Introduction

Autophagy is a catabolic process occurring in all eukaryotic cells so as to maintain cellular viability and homeostasis during basal conditions by controlling long-lived proteins and damaged organelles. Autophagy can also be stimulated to maintain cell survival in response to sublethal stresses, such as nutrient or growth factor deprivation, hypoxia, reactive oxygen species, or viral and pathogen invasion (Choi et al., 2013) This process requires both the ULK1 serine–threonine kinase and the BECLIN 1–VPS34 core complex for its upstream signaling to generate double-membraned vesicles, the autophagosomes, which transfer portions of cytosolic content to lysosomes (Wirth et al., 2013).

ULK1 is one of the most upstream autophagy-related factors; in fact, it forms a stable complex with ATG13, FIP200, and ATG101, playing a crucial role in the initiation steps of autophagy (Noda and Fujioka, 2015). Furthermore, ULK1 regulates its substrates and is itself regulated by phosphorylation events. mTOR and 5′ AMP-activated protein kinase are among its well-known upstream regulators (Kim et al., 2011). Other posttranslational modifications, including ubiquitylation and acetylation, have been reported to modulate the pace of ULK1 turnover and kinase activity in different cellular contexts (Lin et al., 2012; Kuang et al., 2013; Jiao et al., 2015). Indeed, Hsp90 and Cdc37 are chaperones that regulate ULK1 stability and activity by forming a complex with ULK1, which subsequently influences ATG13-mediated mitophagy (Joo et al., 2011). Further, soon after autophagy induction, the stability of ULK1 is regulated by K63-linked ubiquitin chains, which are mediated by the AMBRA1 complex with the E3 ligase TRAF6 (Nazio et al., 2013). Of note, it has been found that AMBRA1 protein levels are also significantly modulated by E3 ligases during the autophagy response (Antonioli et al., 2014; Xia et al., 2014). Several additional E3 ligases have been identified as ULK1 regulators (Nazio et al., 2013; Li et al., 2015; Liu et al., 2016), and it is now apparent that activation of protein kinases can initiate irreversible down-regulation by ubiquitin proteasome system

Correspondence to Francesco Cecconi: cecconi@cancer.dk

Abbreviations used: Act D, actinomycin D; ANOVA, analysis of variance; Baf A1, bafilomycin A1; CHX, cycloheximide; Clq, chloroquine; co-IP, Co-Immunoprecipitation; EBSS, Earle's balanced salt solution; HECT, Homologous to E6AP C terminus; IP, immunoprecipitation; MALDI-TOF/TOF, matrix-assisted laser desorption/ionization time of flight/time of flight; MS, mass spectrometry; Ni-NTA, nickel-nitrilotriacetic acid; oligo, oligonucleotide; qPCR, quantitative real-time PCR; ULK, Unc-51–like kinase; UPS, ubiquitin proteasome system; WB, Western blotting.

The Rockefeller University Press $30.00
J. Cell Biol.
https://doi.org/10.1083/jcb.201605089

Published December 8, 2016

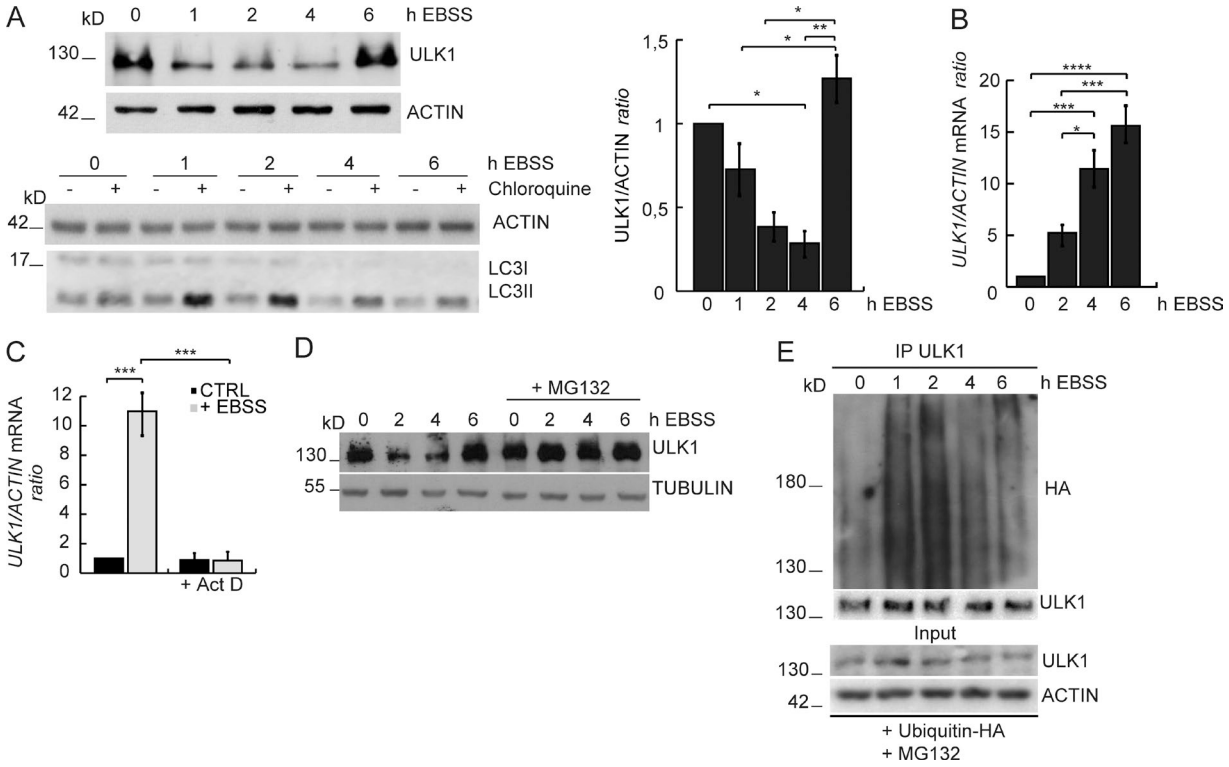

Figure 1. **ULK1 mRNA and protein levels are regulated in a controlled time course during autophagy.** (A) HeLa cells were treated with EBSS for the indicated time periods in the presence or not of Clq, and the levels of ULK1, ACTIN, and LC3 were detected by WB. Densitometric analysis of ULK1 over ACTIN is also shown (right graph). Data are expressed as the mean ± SEM (n = 4). (B) qPCR analysis of *ULK1* mRNA levels in HeLa cells incubated in EBSS medium for the indicated time periods. Data are expressed as mean ± SEM (n = 3). (C) qPCR analysis of *ULK1* mRNA levels in HeLa cells incubated in EBSS medium for 4 h in the presence or not of Act D. Data are expressed as mean ± SEM (n = 3). (D) HeLa cells were treated with EBSS for the indicated time periods in the presence or not of MG132. Protein levels of ULK1 and TUBULIN were detected by WB. (E) HeLa cells were transfected with ubiquitin-HA and treated with EBSS for the indicated time periods in the presence of MG132. Protein extracts were immunoprecipitated in denaturing conditions using an anti-ULK1 antibody; ubiquitin, ULK1, and ACTIN were analyzed by WB. In A and B, data were analyzed by one-way analysis of variance (ANOVA) followed by Tukey post hoc test. *, P < 0.05; **, P < 0.01; ***, P < 0.001; ****, P < 0.0001. In C, data were analyzed by two-way ANOVA followed by Bonferroni's multiple comparison post test. ***, P < 0.001.

(UPS)–mediated protein degradation and that this can be an important mechanism of signal termination (Lu and Hunter, 2009).

Here, we report that ULK1 levels are finely regulated during an autophagy response at the transcriptional, translational, and degradation levels. We show that ULK1 protein is down-regulated during the first few hours of starvation through the activity of the E3 ligase NEDD4L (neural precursor cell-expressed developmentally down-regulated 4–like) and restored to basal levels during prolonged starvation. This ULK1 rescue requires a constant transcription of *ULK1* mRNA and mTOR-dependent de novo protein synthesis reactivation.

mTOR may then inhibit ULK1 activity and block autophagy progression in the absence of new stimuli. Autophagy, if re-induced, can proceed, through this novel pathway of regulation, by tightly controlled pulses, by which a cell can avoid excessive self-digestion culminating in cell death.

Results

ULK1 mRNA and protein levels are regulated in a controlled time course during autophagy

Because the protein levels of AMBRA1, a key regulator of ULK1 protein stability, are regulated by UPS during autophagy (Nazio et al., 2013; Antonioli et al., 2014), we first analyzed ULK1 protein levels in HeLa cells under starvation conditions (lacking both amino acids and serum). We found that ULK1 protein levels are reduced during the first 4 h of starvation, being later restored to almost basal levels after starvation for 6 h (Fig. 1 A). Autophagy flux is analyzed in the presence or absence of the lysosomal inhibitor chloroquine (Clq) by LC3 lipidation. We also analyzed the levels of some ULK1-interacting proteins, such as FIP200 and ATG13. As shown in Fig. S1 A, ATG13 protein levels also decrease during starvation. Moreover, by analyzing the ULK1-dependent phosphorylation of ATG13 (S318), we found an increase in ULK1 kinase activity during the first 2 h of starvation, this being later decreased after starvation for 4–6 h (Fig. S1 A). Such a starvation-induced decrease in ULK1 levels, even though slightly delayed, was also found in HEK293 cells (Fig. S1 B), suggesting that different cell types share this regulation. Next, we decided to analyze *ULK1* mRNA by quantitative real-time PCR (qPCR) during amino acid and serum starvation, and we found that it is greatly increased (by ∼15-fold after 6-h starvation; Fig. 1 B). Furthermore, actinomycin D (Act D), a potent inhibitor of transcription, completely inhibited starvation-induced *ULK1* mRNA up-regulation (Fig. 1 C).

Then, we decided to verify whether the UPS regulates ULK1 protein stability. By treating cells with the proteasome inhibitor MG132 during starvation, we found that ULK1 protein levels increase (Fig. 1 D). Consistently, in the presence of MG132, ULK1 proves to be ubiquitylated during starvation (with this modification showing a rapid increase 1–2 h after

Published December 8, 2016

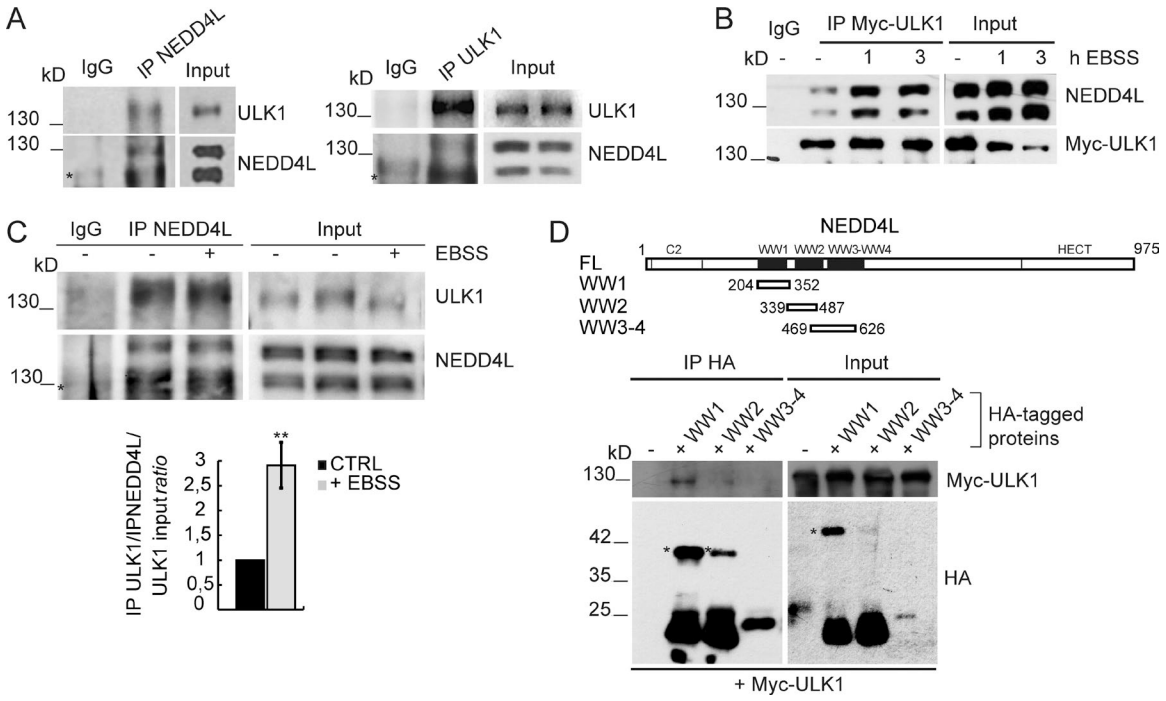

Figure 2. **ULK1 interacts with the E3 ligase NEDD4L.** (A) Protein extracts from HeLa cells were immunoprecipitated using anti-NEDD4L, anti-ULK1 antibodies and with IgG as a negative control. NEDD4L and ULK1 were analyzed by WB. The two NEDD4L bands correspond to two different spliced isoforms. (B) HeLa cells were transiently transfected with Myc-ULK1 and then grown in normal or EBSS medium for 1 and 3 h, respectively. Protein extracts were immunoprecipitated using an anti-Myc antibody or with IgG as a negative control; Myc-ULK1 and NEDD4L were analyzed by WB. (C) HeLa cells were grown either in normal or in EBSS medium for 90 min, respectively. Protein extracts were immunoprecipitated using an anti-NEDD4L antibody or with IgG as a negative control. ULK1 and NEDD4L analyzed by WB. The band density ratio of immunoprecipitated ULK1, relative to immunoprecipitated NEDD4L normalized on the input amount of ULK1, is analyzed ($n = 3$). Data are expressed as the mean ± SD, and statistical analysis was performed using an unpaired Student's *t* test. **, $P < 0.01$. (D) Scheme of NEDD4L full length and fragments showing the N-terminal C2 domain, four WW domains (black boxes), and the HECT domain. HeLa cells were cotransfected with vectors encoding Myc-ULK1 together with NEDD4L-HA fragments encoding the WW1, WW2, and WW3-4 domains, respectively. Protein extracts were immunoprecipitated using an anti-HA antibody; Myc-ULK1 and NEDD4L-HA fragments are analyzed by WB. Asterisk represents unspecific bands.

nutrient starvation), thus suggesting that ULK1 stability is regulated by the proteasome during autophagy (Fig. 1 E).

ULK1 interacts with the E3 ubiquitin ligase NEDD4L

Prompted by this finding, we then moved to the identification of the E3 ubiquitin ligase responsible for the first steps of ULK1 proteasome-dependent degradation. Given the role of TRAF6 on ULK1 positive regulation and our preliminary data on ULK1 interactors based on mass spectrometry (MS) analysis, and because NEDD4L acts as an E3 ligase in the opposite way of TRAF6 in regulating the nerve growth factor receptor TrkA, another kinase and ULK1 interactor (Geetha et al., 2005; Zhou et al., 2007; Georgieva et al., 2011), we decided to investigate the existence of a putative NEDD4L–ULK1 interaction by a biochemical approach. To verify this, coimmunoprecipitation (co-IP) analyses were performed in HeLa cells using both NEDD4L and ULK1 antibodies. These analyses reveal the interaction between endogenous NEDD4L and ULK1 (Fig. 2 A). Moreover, by analyzing the interaction between ULK1 and NEDD4L after autophagy induction by starvation, we found an increase in their binding both in endogenous or overexpression conditions (Fig. 2, B and C). Next, because NEDD4L substrates interact specifically with the WW domains of Homologous to E6AP C terminus (HECT) E3 ligase to be ubiquitylated (Harvey et al., 1999), we tested which NEDD4L WW domains mediate the interaction with ULK1. As shown in Fig. 2 D, the WW1 domain of NEDD4L is capable of binding ULK1, with WW2 showing only a very modest interaction. Unfortunately, no canonical WW-binding PPXY motifs are present in ULK1, suggesting that critical phosphorylated residues could mediate this binding or some adaptor proteins bearing PPXY-like sequences could be involved (Lu et al., 1999; Shearwin-Whyatt et al., 2006; Léon and Haguenauer-Tsapis, 2009).

NEDD4L ubiquitylates ULK1 and induces its degradation via the proteasome

As NEDD4L is a HECT domain–containing E3 ubiquitin ligase, we then tested whether NEDD4L could regulate the protein levels of ULK1. Indeed, wild-type NEDD4L ($NEDD4L^{WT}$) efficiently promotes ULK1 protein decrease, but at variance with its C821A mutant lacking ubiquitin ligase activity ($NEDD4L^{CA}$; Bruce et al., 2008; Yang and Kumar, 2010; Fig. 3, A and B). This effect is specific because overexpression of NEDD4L does not show any effects on other known ULK1-binding proteins, such as ATG13, AMBRA1, and BECLIN 1 (Fig. S2 A). The decrease in ATG13 levels that we find during starvation is therefore most likely regulated by another degradation mechanism.

Because of the high degree of homology between NEDD4 and NEDD4L, and the fact that NEDD4 is involved in the degradation of another key proautophagic protein BECLIN 1 (Platta et al., 2012), we tested whether NEDD4 could also regulate ULK1 protein degradation. However, at variance with NEDD4L, NEDD4 overexpression is not able to induce ULK1 protein decrease (Fig. S2 B).

Published December 8, 2016

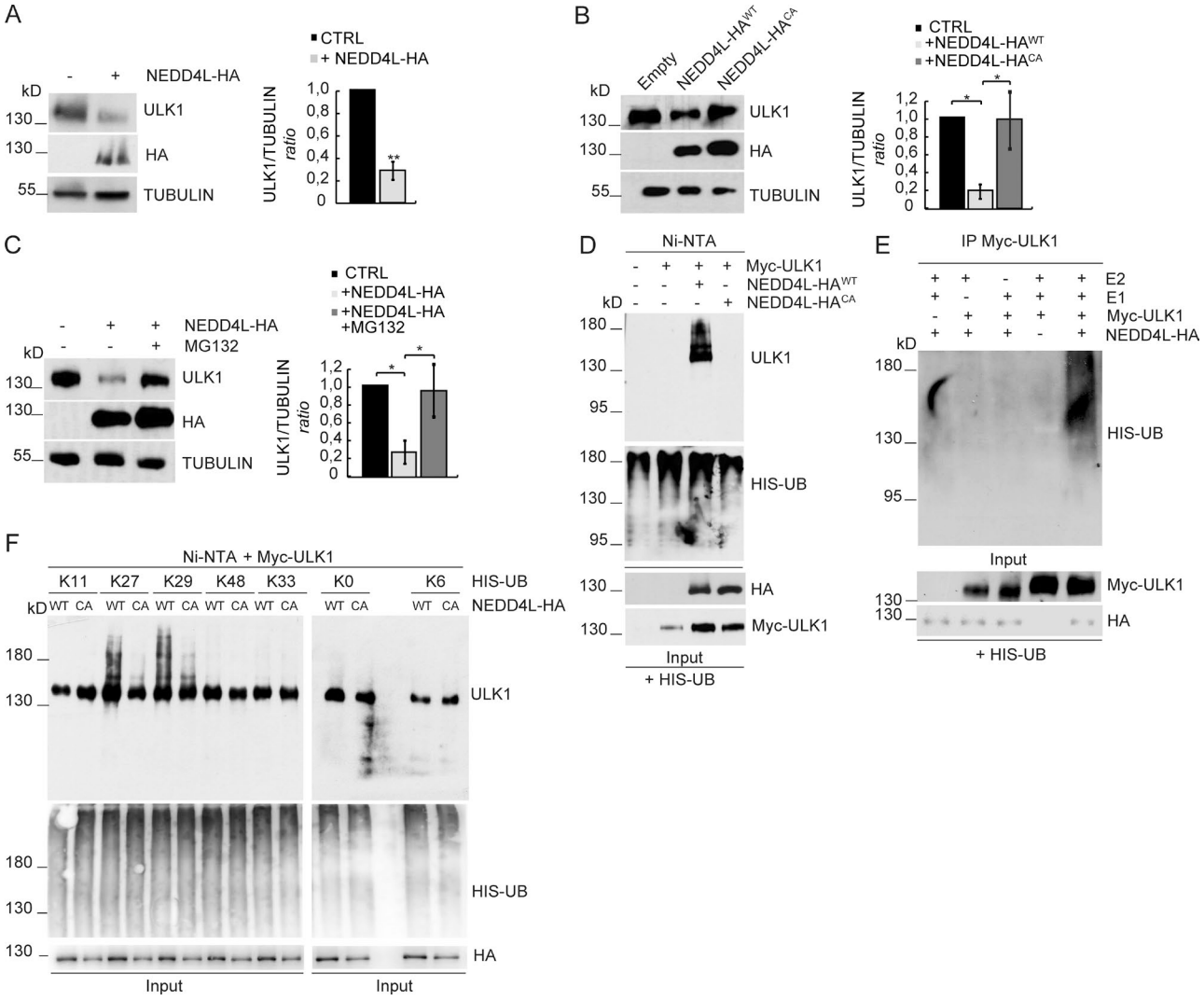

Figure 3. **NEDD4L ubiquitylates ULK1 and induces its degradation via proteasome.** (A) HeLa cells were transfected with empty or NEDD4L-HA vectors; levels of ULK1, NEDD4L, and TUBULIN were detected by WB. Densitometric analysis of ULK1 over TUBULIN is also shown (right graph). Data are expressed as the mean ± SD (n = 3) and statistical analysis was performed using an unpaired Student's t test. **, P < 0.01. (B) HeLa cells were transfected with cDNAs coding for NEDD4L^{WT} and NEDD4L^{CA} HA-tagged proteins; ULK1, NEDD4L, and TUBULIN protein levels were detected by WB. Densitometric analysis of ULK1 over TUBULIN is also shown (right graph). Data are expressed as the mean ± SEM (n = 4). (C) HeLa cells were transfected with NEDD4L-HA in the presence or not of MG132 for 4 h. Levels of ULK1, NEDD4L, and TUBULIN were detected by WB. Densitometric analysis of ULK1 over TUBULIN is also shown (right graph). Data are expressed as the mean ± SEM (n = 3). (D) HeLa cells were cotransfected with a vector encoding a 6xHIS-tag ubiquitin and Myc-ULK1 in combination or not with NEDD4L^{WT} and NEDD4L^{CA} in the presence of MG132. Protein extracts were prepared in a denaturing urea buffer and subjected to Ni-NTA purification. The amount of ubiquitylated Myc-ULK1 copurified with 6xHIS-ubiquitin was evaluated by WB. (E) An in vitro ubiquitylation assay was performed by mixing immunopurified Myc-ULK1 and NEDD4L-HA, together with recombinant HIS-tag ubiquitin. ULK1 ubiquitylation is evaluated using an anti-Ubiquitin antibody to detect the incorporation of recombinant HIS-ubiquitin. The levels of ULK1 and NEDD4L were analyzed by WB. (F) HeLa cells were cotransfected independently with vectors encoding for 6xHIS-tag specific ubiquitin constructs and Myc-ULK1 in combination or not with HA-tagged NEDD4L^{WT} or NEDD4L^{CA} as a negative control. Protein extracts were prepared as in (D) and the amount of ubiquitylated ULK1 copurified with 6xHIS-Ubiquitin was evaluated by WB. The higher expression levels of NEDD4L^{CA} construct are caused by the lack of activity on itself (Bruce et al., 2008). In B and C, data were analyzed by one-way ANOVA followed by Tukey post hoc test. *, P < 0.05.

Next, we found that down-regulation of the ULK1 protein by NEDD4L is blocked by proteasome inhibitors (MG132 and lactacystin), but not by lysosomal inhibitors (leupeptin and Clq; Figs. 3 C and S2 C), indicating that NEDD4L triggers ULK1 degradation exclusively through the proteasome pathway.

Prompted by this finding, we investigated whether NEDD4L could induce ULK1 ubiquitylation. We found that NEDD4L^{WT}, but not NEDD4L^{CA} mutant, efficiently promotes ULK1 ubiquitylation in vivo (Fig. 3 D). To exclude the possibility that NEDD4L might act indirectly on ULK1, we investigated whether NEDD4L could directly ubiquitylate ULK1 in vitro. Indeed, the ubiquitylation assay in vitro reveals a direct ubiquitylation of ULK1 by NEDD4L (Fig. 3 E).

K48-linked ubiquitylation is mainly believed to target substrates for proteasome degradation, whereas K63-linked ubiquitylation is involved in regulating protein activity. It has been reported that NEDD4L is able to promote K11-, K48-, K63-, K29-, K27-, and K6-linked ubiquitylation to mediate the degradation of its substrates (Fotia et al., 2006; Ding et al., 2013). This raised the intriguing question as to what type of degradative ubiquitylation NEDD4L induces on ULK1. To address this, we used a series of HIS-tagged ubiquitin constructs possessing a

Published December 8, 2016

single lysine in the presence of NEDD4L^{WT} or NEDD4L^{CA} as a negative control; as shown in Fig. 3 F, we found that NEDD4L^{WT} promotes noncanonical K27- and K29-linked polyubiquitylation of ULK1. Then, we verified whether ULK1 could be modified by K27- and K29-linked ubiquitin during autophagy; being in ULK1 overexpressing conditions, we analyzed ULK1 ubiquitylation after 4 and 6 h of starvation. As shown in Fig. S2 D, ULK1-linked K27 and K29 ubiquitylation increases after autophagy induction by starvation. Finally, because of the established role in vitro of NEDD4 family members in K63-mediated ubiquitylation (Kim and Huibregtse, 2009; Maspero et al., 2013), we also checked the capability of NEDD4L to promote this kind of modification on ULK1. Indeed, by overexpressing NEDD4L, an increase of K63 ubiquitylation is detectable on ULK1 (Fig. S2 E), implying a putative additional role for ubiquitin K63 chains in regulating ULK1 activity in this context of regulation. Of note, we previously showed that the alternative E3 ligase TRAF6 could favor a similar modification on ULK1 early during autophagy activation (Nazio et al., 2013).

NEDD4L degrades ULK1 protein during prolonged starvation

Given that NEDD4L induces ULK1 proteasomal degradation and that ULK1 is degraded by UPS during starvation, we decided to analyze ULK1 protein levels in cells knocked down for NEDD4L. As shown in Fig. 4 (A–C) and Fig. S3 A, NEDD4L down-regulation induces an increase in ULK1 protein levels in fed conditions and prevents its degradation after prolonged nutrient starvation. Interestingly, we found that ULK2, another Atg1 orthologue in mammals often shown to compensate for ULK1 functions (Alers et al., 2012), also undergoes a similar regulation (Fig. S3 B).

Because ULK1 kinase is active during autophagy induction, we set out to find whether NEDD4L is able to distinguish the active form of ULK1 from the inactive one for the purpose of triggering its proteasomal degradation. We thus cotransfected the cells with three different Myc-tagged ULK1 constructs, the wild-type (ULK1^{WT}), the kinase-dead (ULK1^{K46I}), and the ULK1^{S1047A} (Dorsey et al., 2009) mutated form in its autophosphorylation site (Fig. S3 C) in NEDD4L^{WT}-overexpressing cells, and we analyzed the ability of NEDD4L to degrade and ubiquitylate ULK1. As shown in Figs. 4 D and S3 D, we found that NEDD4L is able to induce the ubiquitylation and subsequently the degradation of only the active form of ULK1, supporting the hypothesis that this regulation occurs specifically upon autophagy.

Moreover, we analyzed the capability of NEDD4L to bind the kinase-dead form of ULK1, and we found that both the wild-type and mutant form of ULK1 are able to interact with NEDD4L (Fig. S3 E), suggesting that ULK1 needs activation to undergo conformational changes functional to its NEDD4L-mediated ubiquitylation, but not to interact with NEDD4L.

Last, because NEDD4L is regulated by self-ubiquitylation (Bruce et al., 2008) and phosphorylation (An et al., 2014), we decided to investigate whether these modifications are regulated during autophagy. First, we analyzed NEDD4L self-ubiquitylation in basal conditions and after autophagy induction by starvation. As shown in Fig. 4 E, NEDD4L displays higher self-ubiquitylation levels after autophagy induction than in control conditions. Next, we noticed that two sites (S342 and S448) flanking the NEDD4L WW domains can be phosphorylated by several AGC kinase family members, including SGK1, Akt, and PKA (Lee et al., 2007; Gao et al., 2009). These phosphorylation events inhibit NEDD4L function as a regulator of ENACs and TGF-β signaling. For this reason, we analyzed the phosphorylation status of NEDD4L during autophagy induction by starvation at different time points. As shown in Fig. 4 F, NEDD4L phosphorylation is reduced during the first 4 h of starvation. Interestingly this modification pattern parallels that of ULK1 expression levels (Fig. 1 A). Moreover, using qPCR, we found a significant increase in *NEDD4L* mRNA during starvation (Fig. 4 G), supporting that NEDD4L is positively regulated during autophagy progression.

Collectively, both of these findings support the hypothesis that NEDD4L is more active during autophagy than in standard conditions, and this facilitates ULK1 proteasomal degradation.

NEDD4L is a negative regulator of autophagy

Based on the evidence that NEDD4L degrades ULK1 during autophagy, we decided to explore whether NEDD4L inactivation, and the resulting stabilization of ULK1 in prolonged starvation, can alter the duration of the autophagy response. To this aim, we down-regulated NEDD4L by RNAi and induced autophagy for different time periods; we then analyzed autophagy using three different methods: LC3 lipidation and p62 protein levels by Western blotting (WB; Fig. 5, A and B) and both LC3 and ATG16L puncta detection by immunofluorescence (Fig. 5, C and D). As shown, in control cells, autophagy rapidly increases at 1–2 h and then declines at 4–6 h of starvation. In NEDD4L-silenced cells, an increased and persistent autophagy flux is observed, suggesting a correlation between ULK1 protein degradation and the on-rate of autophagy.

NEDD4L ubiquitylates ULK1 at lysine 925 and lysine 933

To finely dissect ULK1 regulation by NEDD4L at a structural level, we next determined the NEDD4L-dependent ubiquitylation sites on ULK1. By MS analysis, we identified two lysine residues on the same ULK1 peptide (K925 and K933) that proved to be ubiquitylated (Table S1). By mutating the lysine residues to arginines, we generated three mutant constructs (ULK1^{K925R}, ULK1^{K933R}, and ULK1$^{K925R+K933R}$). First, we analyzed the half-life of the single-mutant constructs in the presence of cycloheximide (CHX), a protein translation inhibitor, or CHX+MG132, and found that the ULK1^{K925R} and ULK1^{K933R} constructs are as active and functional as ULK1^{WT} but more stable than ULK1^{WT} (Fig. 6 A and Fig. S4, A and B).

Then, we evaluated the capability of all the mutant constructs to be degraded by NEDD4L in standard conditions (Fig. 6, B and C) or during autophagy (Fig. 6, D and E), in the presence or not of MG132. We thus found that both mutations affect NEDD4L-dependent degradation of ULK1 during autophagy. Finally, we analyzed the capability of NEDD4L to ubiquitylate ULK1^{K925R}, ULK1^{K933R}, and ULK1$^{K925R+K933R}$ (Fig. 6, F and G) and found a significant decrease in the ubiquitylation status of all the mutant constructs analyzed when compared with the wild type. However, a residual ubiquitylation is found in this context, arguing for the presence for other unknown ubiquitylation site(s).

Because the NEDD4L-dependent ubiquitylation sites are located in the region of ULK1 that is known to mediate the interaction with ATG13 (Jung et al., 2009), we analyzed whether the ULK1-ATG13 binding is affected during autophagy induction

Published December 8, 2016

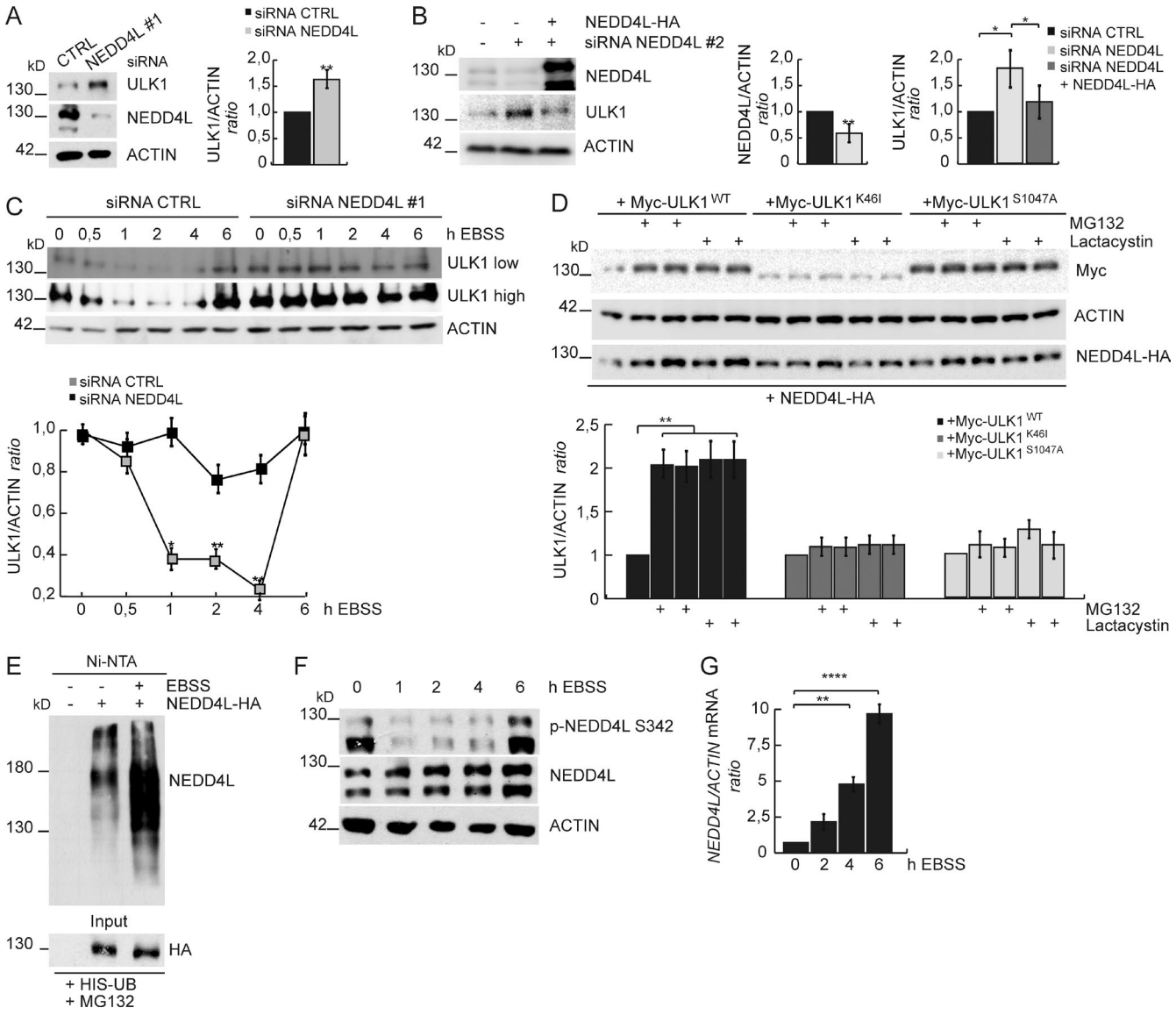

Figure 4. **NEDD4L degrades ULK1 during prolonged starvation.** (A) NEDD4L expression was down-regulated in HeLa cells using specific RNAi oligonucleotides (oligos; siRNA NEDD4L#1) or unrelated oligos as negative control (siRNA CTRL). Densitometric analysis of ULK1 over ACTIN is also shown (right graph). Data are expressed as the mean value ± SD (n = 3), and statistical analysis was performed using an unpaired Student's t test. **, P < 0.01. (B) NEDD4L expression was down-regulated in HeLa cells using specific RNAi oligos targeting NEDD4L 3′UTR (siRNA NEDD4L#2) or unrelated oligos as negative control (siRNA CTRL). Some of them were then transfected with empty vector or NEDD4L-HA. Levels of ULK1, NEDD4L, and ACTIN were detected by WB. Densitometric analyses of both ULK1 and NEDD4L over ACTIN are also shown (right graphs). Data are expressed as the mean value ± SEM (n = 3). (C) NEDD4L expression was down-regulated in HeLa cells as in (A) and autophagy was induced by starving cells for the indicated time periods. Levels of ULK1 and ACTIN were detected by WB. Densitometric analysis of ULK1 over ACTIN is also shown (below graph). Data are expressed as the mean ± SEM (n = 3). Two different expositions (low and high) for ULK1 bands are shown. (D) HeLa cells were cotransfected with cDNAs coding for Myc-tagged ULK1^{WT} or ULK1^{S1047A} or ULK1^{K46I} together with NEDD4L^{WT}-HA in the presence or absence of MG132 or lactacystin for two different time periods (1 h and 2 h). Levels of ULK1, NEDD4L, and ACTIN were detected by WB. Densitometric analysis of ULK1 over ACTIN is also shown (below graph). Data are expressed as the mean ± SEM (n = 3). (E) HeLa cells were cotransfected with a vector encoding 6xHIS-tag Ubiquitin and in some of them with NEDD4L-HA and autophagy was induced for 3 h in the presence of MG132. Protein extracts were prepared in a denaturing urea buffer and subjected to Ni-NTA purification. The amount of ubiquitylated NEDD4L copurified with 6xHIS-ubiquitin was evaluated by WB. (F) HeLa cells were treated with EBSS for the indicated time periods, and the levels of p-NEDD4L, NEDD4L, and ACTIN were detected by WB. (G) qPCR analysis of *NEDD4L* mRNA levels in HeLa cells incubated in EBSS medium for the indicated time periods. Data are expressed as mean ± SEM (n = 3). In B–D and G, data were analyzed by one-way ANOVA followed by Tukey post hoc test. *, P < 0.05; **, P < 0.01; ****, P < 0.0001.

or after NEDD4L overexpression. As shown in Fig. S4 (C and D), no impairment is found, suggesting that ATG13–ULK1 binding is not necessary for ULK1 degradation.

Finally, we decided to analyze autophagy in the presence of ULK1 mutant constructs. Thus, we expressed, in independent experiments, ULK1^{WT} and ULK1$^{K925R+K933R}$ mCherry-tagged plasmids in ULK1 knockdown cells, and we analyzed ATG16L puncta formation after autophagy induction by starvation at two different time points. As shown in Figs. 6 H and S4 E, the ULK1 mutant construct increases autophagy with respect to the ULK1^{WT}, as we found after NEDD4L down-regulation. A similar autophagy alteration is also found by only increasing ULK1 levels by expression of ULK1^{WT} or ULK1$^{K925R+K933R}$ in control cells (Fig. S4 F). Moreover, also using the single-mutant

Published December 8, 2016

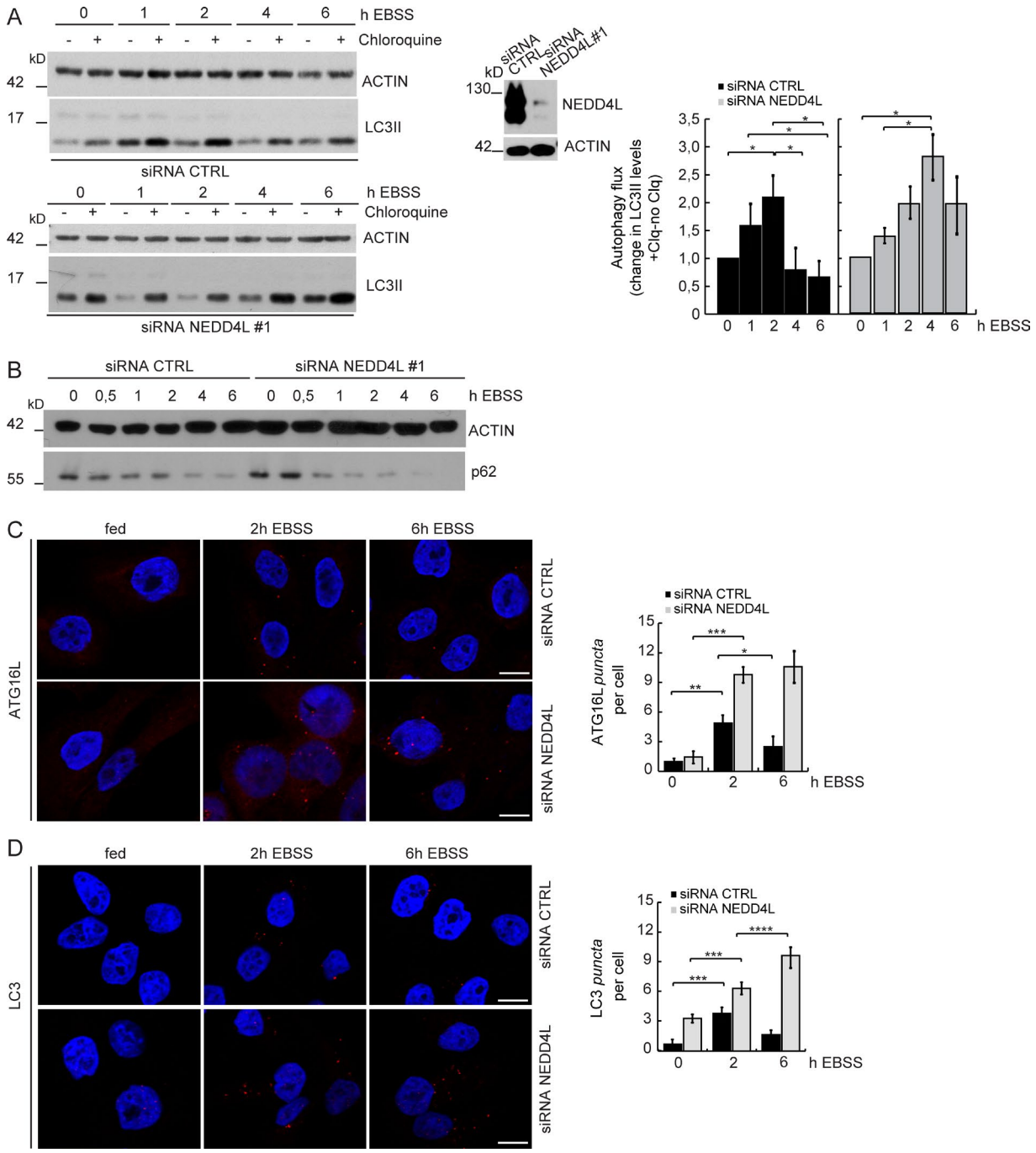

Figure 5. **NEDD4L down-regulation increases autophagy.** (A) NEDD4L expression was down-regulated in HeLa by RNAi. Cells were nutrient-starved for the indicated time periods in the presence or not of Clq. Protein extracts were analyzed by WB for the expression of LC3, ACTIN, and NEDD4L. Densitometric analysis of LC3II+Clq-LC3II control over ACTIN band is shown. Data are expressed as the mean ± SEM of three independent experiments ($n = 3$). (B) HeLa cells were treated as in A. Protein extracts were analyzed by WB for the expression of p62 and ACTIN. (C and D) NEDD4L expression was down-regulated by RNAi as in A; cells were nutrient-starved for the indicated time periods and fixed and labeled with anti-ATG16L or anti-LC3 antibodies (red puncta) and visualized by confocal microscopy. Analysis of the number of both ATG16L and LC3 puncta occurrence per cell is shown in the graph. Data are expressed as the mean ± SEM ($n = 3$); representative images are shown. Bar, 20 µm (>50 cells analyzed per sample). In A, data were analyzed by one-way ANOVA followed by Tukey post hoc test. *, $P < 0.05$. In C and D, data were analyzed by two-way ANOVA followed by Bonferroni's multiple comparison post test. *, $P < 0.05$; **, $P < 0.01$; ***, $P < 0.001$; ****, $P < 0.0001$.

constructs (ULK1^{K925R} and ULK1^{K933R}), LC3 lipidation is increased and stable during the starvation period (Fig. S4 G). Further, this effect is not additive to NEDD4L down-regulation (Fig. S4 H). All these experiments support the idea that there is a correlation between ULK1 protein degradation and termination of the autophagy response.

ULK1 restoration requires de novo mTOR-dependent protein synthesis

Last, we investigated the mechanism underlying the restoration of ULK1 during prolonged starvation. Because it is known that mTOR is reactivated during prolonged starvation (Yu et al., 2010; Sahani et al., 2014) and its activity also reported as

Published December 8, 2016

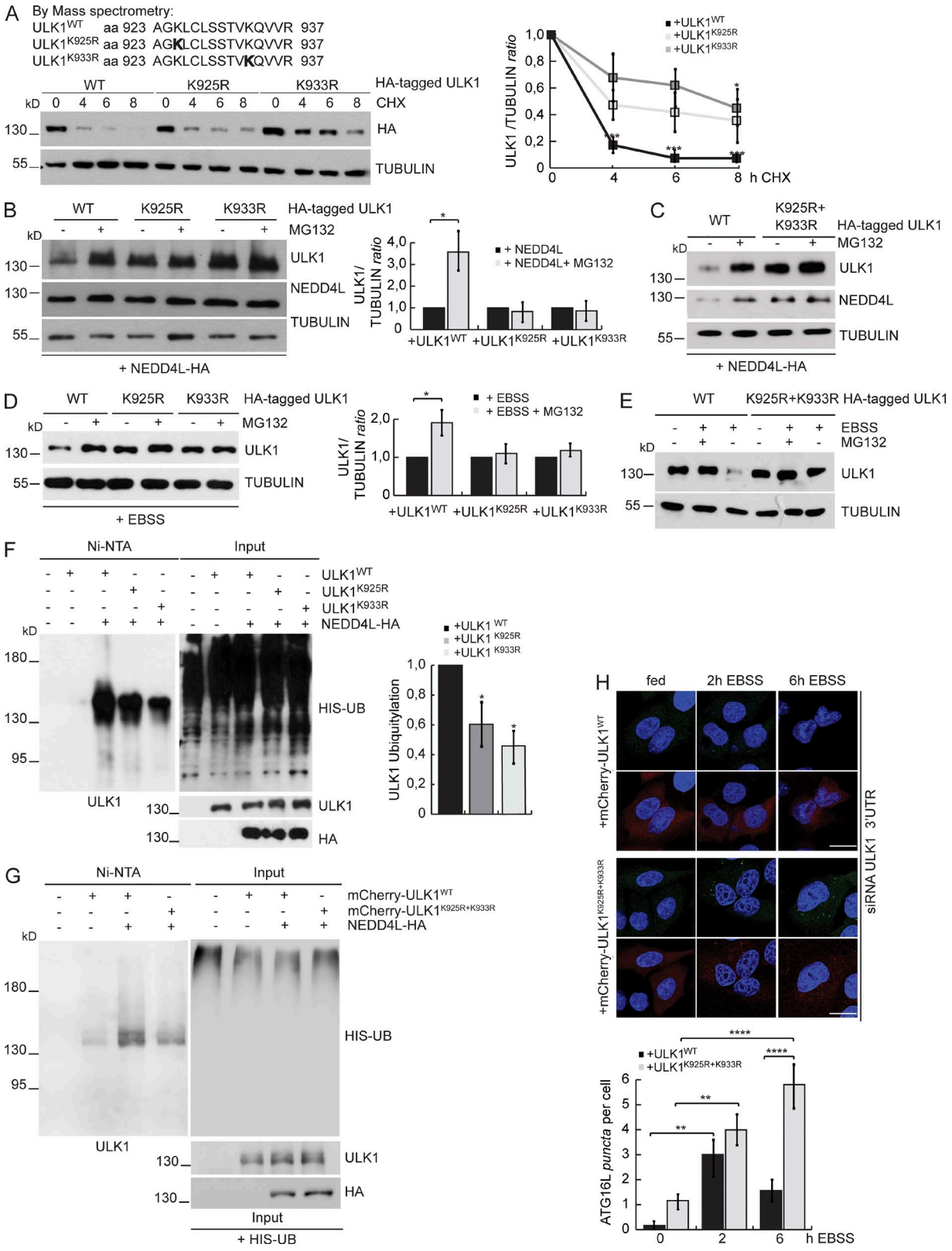

Figure 6. **NEDD4L ubiquitylates ULK1 at lysine 925 and lysine 933.** (A) HeLa cells were transfected with ULK1^{WT}, ULK1^{K925R}, and ULK1^{K933R} HA-tagged proteins and treated with CHX (50 µM) for different time periods. Levels of ULK1 and TUBULIN were detected by WB. Densitometric analysis of ULK1 over TUBULIN is also shown (right graph). Data are expressed as the mean ± SEM (n = 3). (B and C) HeLa cells were transfected ULK1^{WT}, ULK1^{K925R}, ULK1^{K933R}, and ULK1$^{K925R+K933R}$ HA-tagged proteins together with NEDD4L-HA in the presence or not of MG132 (4 h) and all were treated with CHX for 3 h. Levels of ULK1, NEDD4L, and TUBULIN were detected by WB. (B) Densitometric analysis of ULK1+MG132/ULK1 control over TUBULIN bands is also shown. Data are expressed as the mean ± SEM (n = 3). (D and E) HeLa cells were transfected with ULK1^{WT}, ULK1^{K925R}, ULK1^{K933R}, and ULK1$^{K925R+K933R}$ HA-tagged proteins in the presence or not of MG132 and autophagy was induced with EBSS for 4 h. The levels of ULK1 and TUBULIN were detected by WB.

Published December 8, 2016

oscillatory in lymphocytic subpopulation in response to proliferative stimuli (Procaccini et al., 2010), we first analyzed the involvement of mTOR kinase.

As shown in Fig. 7 A and Fig. S5 A, mTOR is active after 6 h with both amino acid and serum starvation or with amino acid alone. We analyzed both the autophosphorylation of mTOR and the mTOR-mediated phosphorylation of ULK1 and found that the newly synthesized pool of ULK1 is directly inhibited by mTOR phosphorylation, contributing to maintain autophagy inhibition after prolonged starvation. Next, when cells were treated with two different mTOR inhibitors, rapamycin and Torin1 at 4 h of starvation, we found that mTOR inhibition effectively suppressed both ULK1 protein level restoration and ULK1 neophosphorylayion by mTOR (Fig. 7, B and C), suggesting an involvement of mTOR reactivation in ULK1 restoration. Then, to evaluate whether the restoration of ULK1 required de novo protein synthesis, we used CHX after 4 h of starvation and found that this treatment also abolished ULK1 restoration, even though CHX is known to secondarily activate mTOR (Fig. 7 C).

Because we found an increase in *ULK1* mRNA level transcription during autophagy (Fig. 1 B), we analyzed whether transcriptional up-regulation was required for ULK1 protein restoration. As shown in Fig. 7 D, Act D is able to inhibit ULK1 restoration after 6 h of starvation, supporting the role of *ULK1* mRNA transcription as propaedeutical for de novo synthesis of ULK1 protein.

To determine whether increased translation of *ULK1* mRNA accounted for the increased protein levels at 6 h of starvation, we performed sucrose gradients to profile ULK1 mRNA distribution in translationally active polysomes or in translationally inactive RNPs (Bianchini et al., 2008). Autophagy was induced by starvation for 2 and 6 h, and polysome–mRNA complexes were fractionated by sucrose gradient centrifugation. Figs. 7 E and S5 B show a decrease in polysome-associated *ULK1* mRNA in cells grown under starvation conditions for 2 h, indicating translational repression of the mRNA. However, a strong recruitment of *ULK1* mRNA was observed after 6 h of starvation, strongly suggesting that increased translation of *ULK1* mRNA at 6 h of starvation (after mTOR reactivation) contributes to de novo synthesis of ULK1 protein.

Because prolonged autophagy is known to influence cell death (Füllgrabe et al., 2013; Antonioli et al., 2014), we analyzed cell viability in both control conditions and after NEDD4L down-regulation during prolonged starvation and in the presence or not of a low dose of bafilomycin A1 (Baf A1). As shown in Figs. 7 F and S5 C, when NEDD4L is down-regulated and autophagy remains high, we can detect an increase in starvation-induced cell death, which is blocked by Baf A1, suggesting that persistent autophagy may trigger cell demise.

Autophagy restimulation requires mRNA preaccumulation and is amplified by NEDD4L down-regulation

To gain insight into the physiological relevance of ULK1 protein and mRNA modulation during prolonged starvation, we first decided to analyze ULK1 protein levels after reinduction of autophagy in the system by nutrient replenishment. As shown in Fig. 8 A, ULK1 protein levels can be down-regulated again as soon as autophagy is reinduced, indicating an oscillating regulation for this autophagy key factor. Then, to evaluate the importance of mRNA transcription in general (and of *ULK1* mRNA in particular; Fig. 1 D) in this oscillation, we used Act D for the first 4 h of starvation and analyzed both ULK1 protein levels and autophagy occurrence. As shown in Fig. 8 B, the temporary inhibition of mRNA transcription is sufficient to block autophagy reinduction by starvation after nutrient replenishment, as analyzed by counting ATG16L puncta. On the contrary, when NEDD4L is down-regulated and ULK1 protein levels cannot be decreased, we observed a stronger reinduction of autophagy (Fig. 8 C) when compared with the control. These results, collectively, confirm the importance of ULK1 fine-tuning in autophagy restimulation, which confers an oscillatory behavior to autophagy progression.

Discussion

Autophagy is the last resource to help cells survive during starvation, but self-degradation has a limit, beyond which the cell will die. For instance, after birth, in neonatal tissues, a rapid reprogramming of cell metabolism is necessary, and autophagy is activated soon after the transplacental nutrient supply is suddenly interrupted. However, autophagosome formation after birth is completely prevented, suggesting that neonates use the amino acids produced by autophagy for energy homeostasis (Schiaffino et al., 2008).

Displaying a negative control mechanism will thus help cells avoid overactivation of autophagy, enabling them to calibrate autophagy to an optimal level and ensuring that they can survive prolonged starvation. In fact, this study supports a mechanism of cross-regulation of *ULK1* mRNA transcription, protein translation, and degradation in response to the oscillatory activation of mTOR that regulates autophagy induction (see our model in Fig. 9). It is well known that the mTOR pathway activity is also regulated by oscillation in other contexts, such as in regulatory T cell proliferation, where another proautophagic

(D) Densitometric analysis of ULK1+MG132/ULK1 control over TUBULIN bands is also shown. Data are expressed as the mean ± SEM (n = 3). (F) HeLa cells were transfected with a vector encoding a 6xHIS-tag ubiquitin together with ULK1^{WT}, ULK1^{K925R} and ULK1^{K933R} HA-tagged proteins in the presence of NEDD4L. Protein extracts were prepared in a denaturing urea buffer and subjected to Ni-NTA purification. The amount of ubiquitylated ULK1 copurified with 6xHIS-ubiquitin was valuated by WB. The intensity of ULK1 bands is shown. Data are the mean ± SEM (n = 3). (G) HeLa cells were transfected with a vector encoding a 6xHIS-tag ubiquitin together with ULK1^{WT} and ULK1$^{K925R+K933R}$ mCherry-tagged proteins in the presence of NEDD4L. Protein extracts were prepared in a denaturing urea buffer and subjected to Ni-NTA purification. The amount of ubiquitylated ULK1 copurified with 6xHIS-ubiquitin was evaluated by WB. (H) Endogenous ULK1 was silenced by RNAi; cells were then transfected with ULK1^{WT} or ULK1$^{K925R+K933R}$ mCherry-tagged plasmids. Cells were nutrient-starved for the indicated time periods, fixed and labeled with anti-ATG16L antibody (green puncta), and visualized by confocal microscopy. Analysis of the number of ATG16L occurrence per cell is shown in the graph. Data are expressed as the mean value± SEM (n = 3). Representative images are shown. Bars, 20 µm (>50 cells analyzed per sample). In A, B, D, and F, data were analyzed by one-way ANOVA followed by Tukey post hoc test. *, $P < 0.05$; ****, $P < 0.0001$. In H, data were analyzed by two-way ANOVA followed by Bonferroni's multiple comparison post test. **, $P < 0.01$; ****, $P < 0.0001$. For all ULK1 mutant constructs the same amount of DNA is used for the transfection; the differences are caused by the increased stability of these mutants.

Published December 8, 2016

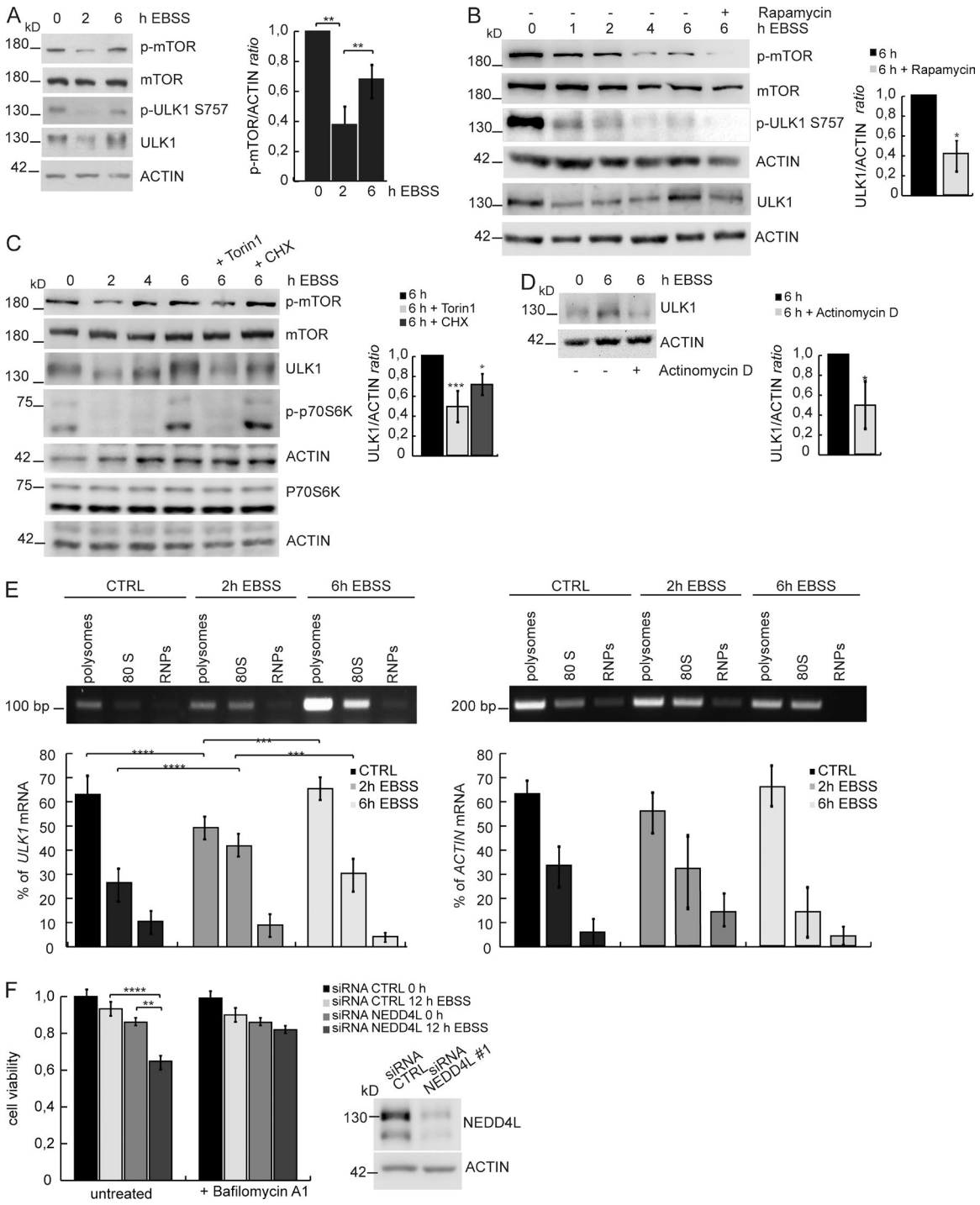

Figure 7. **ULK1 restoration requires de novo mTOR-dependent protein synthesis.** (A) HeLa cells were treated with EBSS for the indicated time periods. The levels of p-mTOR, mTOR, ULK1, p-ULK1 S757, ULK1, and ACTIN were detected by WB. Densitometric analysis of p-mTOR over ACTIN is also shown (right graph). Data are expressed as the mean ± SEM (n = 4). (B) HeLa cells were treated with EBSS for the indicated time periods; at 4 h of starvation, rapamycin (100 nM) was added. Levels of p-mTOR, mTOR, ULK1, p-ULK1 S757, and ACTIN were detected by WB. Densitometric analysis of ULK1 over ACTIN is also shown (right graph). Data are expressed as the mean ± SD (n = 3), and statistical analysis was performed using unpaired Student's t test. *, P < 0.05. (C) HeLa cells were treated with EBSS for the indicated time periods and at 4 h of starvation, 250 nM Torin1 or 50 µM CHX was added. Levels of p-mTOR, mTOR, p-p70S6K, ULK1, and ACTIN were detected by WB. (D) HeLa cells were treated with EBSS for 6 h in the presence or not of Act D. Levels of ULK1 and ACTIN were detected by WB. Densitometric analysis of ULK1 over ACTIN is also shown (right graph). Data are expressed as the mean ± SD (n = 3) and statistical analysis was performed using unpaired Student's t test. *, P < 0.05. (E) qPCR analysis of polysomal recruitment of *ULK1* and *ACTIN* mRNAs in control (CTRL) and EBSS-starved (2 h EBSS and 6 h EBSS) HeLa cells. Densitometric analysis of the signal in each fraction was performed, and the results were represented as the percentage of total signal in all fractions. Data represent mean ± SEM (n = 3). (F) NEDD4L expression was down-regulated by RNAi. Cells were nutrient-starved for 12 h in the presence or not of Baf A1 and analyzed by MTS assay. NEDD4L down-regulation was detected by WB. In A and C, data were analyzed by one-way ANOVA followed by Tukey post hoc test. *, P < 0.05; **, P < 0.01; ***, P < 0.001. In E and F, data were analyzed by two-way ANOVA followed by Bonferroni's multiple comparison post test. ***, P < 0.001; ****, P < 0.0001.

Published December 8, 2016

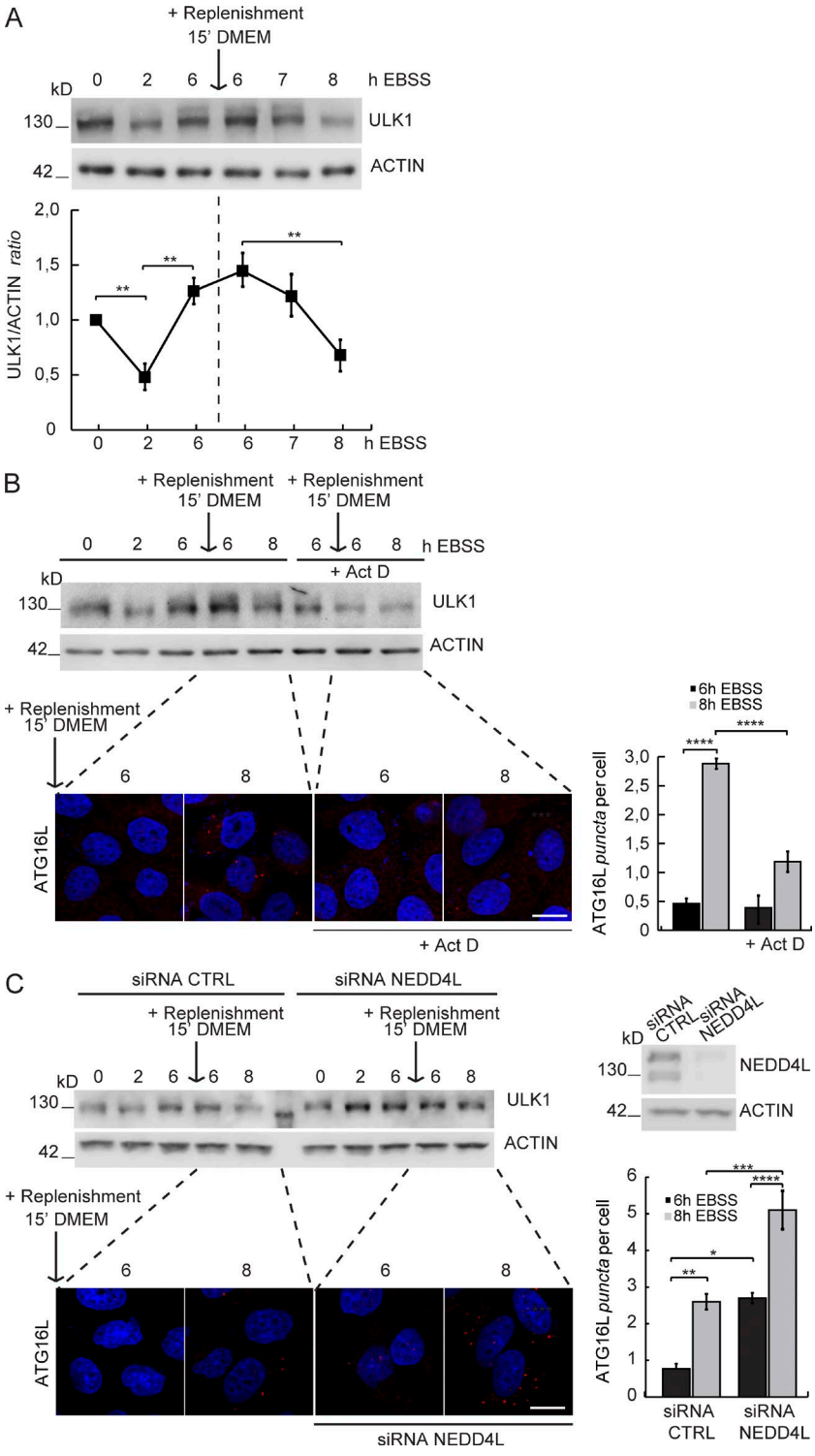

Figure 8. **Autophagy restimulation requires mRNA preaccumulation and is amplified by NEDD4L down-regulation.** (A) HeLa cells were treated with EBSS for the indicated time periods. After 6 h, in some samples, full medium was added for 15 min, and then cells were starved again for 1 and 2 h, respectively. Protein levels of ULK1 and ACTIN were detected by WB. Densitometric analysis of ULK1 over ACTIN is also shown (below graph). Data are expressed as the mean ± SEM (n = 3). (B) HeLa cells were treated with EBSS as in A. In some samples, Act D was added for the first 4 h of starvation. Then, cells were analyzed both by WB and by immunofluorescence. Protein levels of ULK1 and ACTIN were detected by WB. ATG16L puncta occurrence (red puncta) was visualized by confocal microscopy. Analysis of the number of ATG16L puncta per cell is shown in the graph. Data are expressed as the mean ± SEM (n = 3); representative images are shown. Bar, 20 µm (>50 cells analyzed per sample). (C) NEDD4L expression was down-regulated in HeLa cells by using specific RNAi oligos (siRNA NEDD4L#1) or unrelated oligos as a negative control (siRNA CTRL). Cells were nutrient-starved as in A. Protein extracts were next analyzed by WB for the expression of ULK1, NEDD4L, and ACTIN. ATG16L puncta occurrence (red puncta) was visualized by confocal microscopy. Analysis of the number of ATG16L puncta per cell is shown in the graph. Data are expressed as the mean ± SEM (n = 3); representative images are shown. Bar, 20 µm (>50 cells analyzed per sample). Data represent mean ± SEM (n = 3). In A, data were analyzed by one-way ANOVA followed by Tukey post hoc test. **, $P < 0.01$. In B and C, data were analyzed by two-way ANOVA followed by Bonferroni's multiple comparison post hoc test. *, $P < 0.05$; **, $P < 0.01$; ***, $P < 0.001$; ****, $P < 0.0001$.

stimulus, the mTOR inhibitor rapamycin, might differentially affect regulatory T cells reactivity depending on their metabolic state (Procaccini et al., 2010). Moreover, the *ULK1* gene has been found to be a target of C/EBPβ protein, a transcription factor that links autophagy to the circadian pacemaker and maintains nutrient homeostasis throughout light/dark cycles; this is consistent with the fact that autophagy is highly sensitive to nutritional status (Ma et al., 2011). In sum, ULK1 complex regulation may represent a hinge point in a cell response to stress, and its oscillatory nature, intended as the key to the remitting and relapsing nature of autophagy, can be considered as an essential element of the cell's struggle between death and survival.

NEDD4L is an ubiquitin ligase implicated in several cellular or physiological processes (Goel et al., 2015). It is known that two members of the NEDD4 family, NEDD4 and SMURF1 (SMAD-specific E3 ubiquitin protein ligase 1), are involved in autophagy. NEDD4 has been found to promote BECLIN 1 degradation by the proteasome (Platta et al., 2012). Further, RNAi analyses revealed that NEDD4 down-regulation leads to an autophagy increase (Behrends et al., 2010). SMURF1

Published December 8, 2016

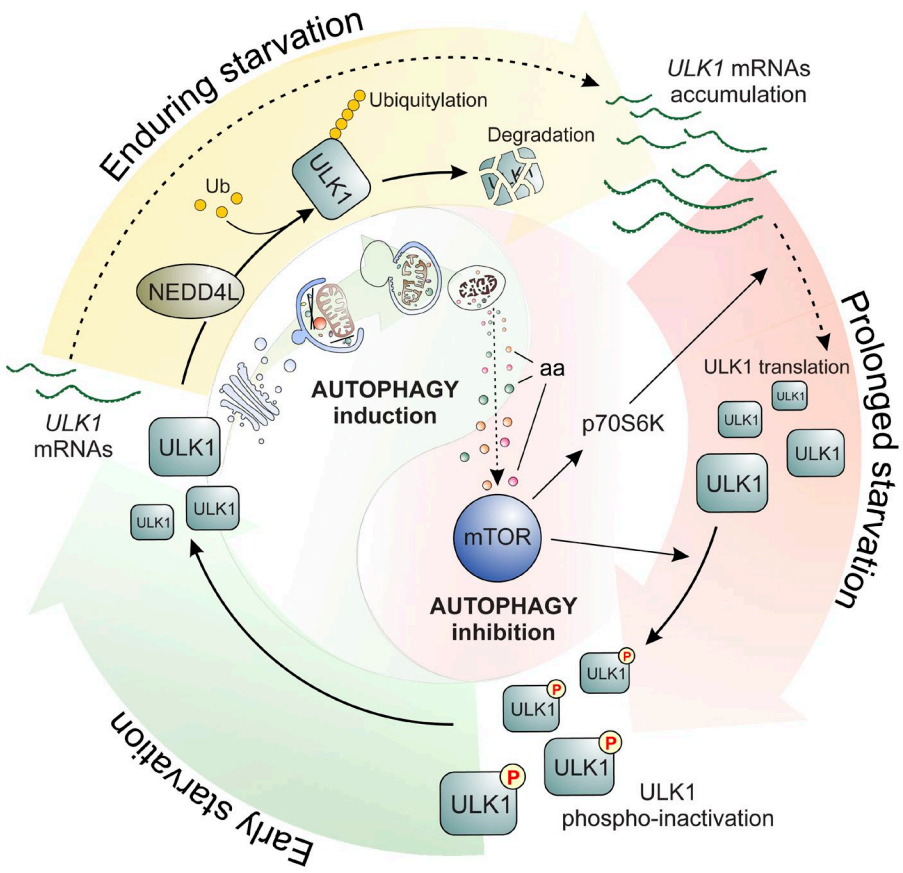

Figure 9. **A cyclic scheme representing autophagy oscillatory regulation.** (A) In enduring starvation, NEDD4L promotes ULK1 degradation while *ULK1* mRNA is actively transcribed. When the autophagy recycling activity makes more nutrients available for protein synthesis, mTOR is reactivated (in conditions of prolonged starvation), and ULK1 mRNA is actively translated upon p70S6K phosphorylation. Then the mTOR kinase function inhibits again the ULK1 protein by phosphorylation, thus making the system ready to respond a putative new stimulus (early starvation), capable to reactivate autophagy. This regulation allows oscillatory autophagy behavior, both preventing excessive autophagy and preparing the cell for a prompt autophagy response upon its reinduction.

plays multiple physiological functions through targeting a variety of substrates acting in both viral autophagy and mitophagy (Orvedahl et al., 2011).

We previously described ubiquitylation of ULK1 by a K63-linked chain mediated by the TRAF6–AMBRA1 complex during short-term starvation and at early time points (30 min), an event stabilizing the active ULK1 complex (Nazio et al., 2013). In a recent paper, we found that the other autophagy activator and ULK1 regulator AMBRA1 is degraded by the Cullin4–DDB1 complex during prolonged starvation and that AMBRA1–TRAF6 binding to ULK1 decreases during prolonged autophagy (Antonioli et al., 2014). An obvious hypothesis is that when the AMBRA1–TRAF6 complex dissociates from ULK1, the ULK1 carboxy-terminal domain becomes unmasked and available for NEDD4L-dependent ubiquitylation.

Moreover, the NEDD4L-mediated ULK1 ubiquitylation is reminiscent of another target of TRAF6 and NEDD4L ligases, TrkA; TRAF6-dependent ubiquitylation is supposed to function nonproteolytically, whereas NEDD4L-mediated ubiquitylation results in the degradation of this plasma membrane receptor (Geetha et al., 2005; Georgieva et al., 2011). We can thus speculate that, similarly to TrkA, ULK1 can be alternatively regulated by these two ligases with two opposite effects, implicating the existence of an ULK1-targeting E3 ligase network regulating cell fate. Last, the recent finding that Cullin3–KHLH20 can also degrade ULK1, Beclin 1, and Vps34 during prolonged autophagy may reflect the need for the cell to possess alternative backup systems for autophagy termination, highlighting the absolute need for a tight control of this event in the general cellular homeostasis (Liu et al., 2016).

As a matter of fact, E3 ligases can promote the formation of polyubiquitin chains on substrates through any of the seven lysines present on ubiquitin molecules. Interestingly, the NEDD4L-mediated ubiquitylation of ULK1 is K27- and K29-linked, but not typical K48-linked, ubiquitylation. Our finding adds to the recent and relatively small amount of existing data on this type of posttranslational modification.

A final issue of interest is the fact that NEDD4L is able to regulate autophagy also in basal conditions. Although basal autophagy has been shown to be independent of ULK1 in a few instances (Petherick et al., 2015; Joo et al., 2016), this does not seem to be the case in cancer cell lines that are characterized by a strong basal autophagy, including HeLa cells (Mizushima, 2010; Wong et al., 2015). Indeed, we found that NEDD4L interacts with ULK1 also in basal conditions and also when the ULK1 kinase domain is disrupted. However, NEDD4L is able to degrade only activated ULK1. Several general principles apply to the degradation of activated protein kinases or their regulators for ubiquitylation and degradation (Lu and Hunter, 2009). Autophosphorylation of ULK1 could change its conformation for NEDD4L-mediated ubiquitylation or, alternatively, the NEDD4L pool binding ULK1 in the absence of autophagy induction is in an inactive form. The trans-phosphorylation of a protein kinase could, indeed, create a phosphodegron that is necessary for ubiquitylation by a phospho-dependent ligase, such as NEDD4L. In addition, because phosphorylation on S342 of NEDD4L is necessary for its subsequent ubiquitylation activity (Lee et al., 2007; Gao et al., 2009), ULK1 could also be involved in regulating other kinases (such as SGK1, Akt, and PKA) known to phosphorylate the NEDD4L residue S342.

Published December 8, 2016

A comprehensive analysis of the autophagy-related posttranslational modifications is therefore of the highest importance in biomedicine and may represent the forefront of autophagy research.

Materials and methods

Cell culture and autophagy assays

HeLa and HEK293 cells were cultured in DMEM (Sigma-Aldrich) supplemented with 10% FBS (Sigma-Aldrich), 2 mM L-glutamine, and 1% penicillin/streptomycin solution at 37°C under 5% CO_2.

The induction of autophagy by nutrients starvation was obtained washing the cells with PBS and incubating them with Earle's balanced salt solution (EBSS; Sigma-Aldrich). Proteasome activity was inhibited for indicated time points with 5 µM MG132 (Sigma-Aldrich) and 20 µM lactacystin; lysosome activity was inhibited for 1 h with 20 µM Clq (added for the last hour of the treatment; Sigma-Aldrich), 10 µM leupeptin (Sigma-Aldrich), or 10 nM Baf A1, and autophagy was induced with 100 nM rapamycin (Sigma-Aldrich) or 250 nM Torin1 (Tocris Bioscience). Transcription was inhibited with 0.5 µM Act D (Sigma-Aldrich). HeLa cells were transiently transfected with Lipofectamine 2000 (Thermo Fisher Scientific) as provided by the supplier.

Ni-NTA assay

For detection of whole-cell ubiquitylation, HeLa cells were transfected with a 6×HIS-ubiquitin expression plasmid along with equal amounts of the indicated plasmids. Thereafter, cells were collected in PBS, resuspended in 1 ml lysis buffer (8 M urea, 0.1 M NaH_2PO_4, 0.05 M Tris, pH 8.0, 40 mM imidazole, 0.5% CHAPS, and 50 mM 2-chloroacetamide), sonicated, and centrifuged. To lysates containing equal amounts of whole-cell protein, 30 µl nickel-nitrilotriacetic acid (Ni-NTA) beads (QIAGEN) were added, and the mixture was incubated at room temperature for 4 h with rotation. Subsequently, the beads were washed for 5 min at room temperature with 800 µl lysis buffer containing 40 mM imidazole. Ubiquitylated proteins were eluted by incubating the beads in 30 µl buffer containing 400 mM imidazole and 2× Laemmli buffer and resolved by SDS-PAGE followed by immunoblotting with the indicated antibodies.

In vitro ubiquitylation assays

HeLa cells were independently transfected with plasmids encoding NEDD4L-HA and Myc-ULK1. 24 h later, cells were lysed in buffer (20 mM Hepes, pH 7.4, 2 mM EGTA, 50 mM M glycerophosphate, 0.5% Triton X-100, 0.5% CHAPS, and 10% glycerol) containing protease inhibitors. Lysates were cleared by centrifugation and subjected to IP using agarose-coupled antibodies against HA or Myc tags. After lysis and before IP, 1% SDS was added and the lysates were incubated for 5 min at 90° to dissociate protein–protein interactions. The samples were diluted 10-fold with the same buffer and the IP assay was performed as previously described. NEDD4L-HA was eluted using 300 mg/ml HA peptide (Sigma-Aldrich). The assays were performed in a 20-µl reaction volume combining the immunopurified proteins and the following recombinant components: 0.2 µg Ube1 (Boston Biochem), 0.5 µg UbcH5b (Boston Biochem), and 100 µM HIS-ubiquitin (Boston Biochem). The reaction was performed at 30°C for 1 h with agitation. The incorporation of ubiquitin was analyzed by WB using an antibody against the ubiquitin.

Plasmids

Plasmids encoding for wild-type ULK1-Myc, ULK1-K46I, and wild-type ULK1-HA were provided by S.A. Tooze (The Francis Crick Institute, Lincoln's Inn Fields Laboratories, London, England, UK). NEDD4L-HA^{WT} and NEDD4L-HA^{CA} plasmids were from Addgene. J. Massaguè (Memorial Sloan Kettering Cancer Center, New York, NY) provided NEDD4L deletion constructs. ULK1 mutant constructs were generated by using the site-directed mutagenesis kit (Agilent Technologies). The sequences used are as follows: K925R, 5′-GACCAGATCCGGGCCGGCAGGCTCTGC CTGTCGTCCACTGTG-3′; K933E, 5′-CTGCCTGTCGTCCACTGT GAGGCAGGTGGTGCGCAGGCTGAATG-3′; S1047A, 5′-GACTCT CGGCCCTGCTGGCTGGTGTCTATGCCTGA-3′.

Antibodies

The primary antibodies used in this study were: mouse and rabbit anti–HA tag antibody (Sigma-Aldrich), mouse anti-Myc (Santa Cruz Biotechnology, Inc.), rabbit anti–BECLIN 1 (Santa Cruz Biotechnology, Inc.), rabbit anti-LC3 (Cell Signaling Technology), rabbit anti–human AMBRA1 (Novus Biologicals), mouse anti-multiubiquitin (MBL), rabbit anti-ULK1 (Santa Cruz Biotechnology, Inc.), goat anti-ULK1 (Santa Cruz Biotechnology, Inc.), rabbit anti-pS757 ULK1 (Cell Signaling Technology), mouse anti-ULK2 (Abcam), rabbit anti-NEDD4L (Cell Signaling Technology), mouse anti-NEDD4L (Santa Cruz Biotechnology, Inc.), rabbit anti-pS342 NEDD4L (Cell Signaling Technology), rabbit anti-mTOR (Cell Signaling Technology), rabbit p-S2448 mTOR (Cell Signaling Technology), rabbit anti-p62 (Santa Cruz Biotechnology, Inc.), rabbit anti-ATG13, rabbit p-S318 ATG13 (Rockland), rabbit anti-Actin (Sigma-Aldrich), mouse anti-Tubulin (Sigma-Aldrich), rabbit cleaved-PARP (Cell Signaling Technology), rabbit anti-Atg16L (Cell Signaling Technology), and rabbit p-p70S6K and p70S6K (Cell Signaling).

Immunoprecipitation and WB

HeLa cells were rinsed with ice PBS and lysed in CHAPS lysis buffer (40 mM Hepes, pH 7.4, 2 mM EDTA, 0.3% CHAPS, and protease and phosphatase inhibitor cocktail; Sigma-Aldrich). 0.5 mg lysates for co-IP in overexpression and 2 mg lysates for co-IP in endogenous conditions were then incubated with 2 µg primary antibody for ULK1 and NEDD4L or 1 µg primary antibody for MYC at 4°C with rotation overnight before addition of 30 µl protein A agarose beads (Roche) and then incubated at 4°Ψ for 1 h.

For the co-IP of HA-tagged proteins, lysates were incubated with 20 µl agarose-coupled antibodies against HA at 4°Ψ for 2 h.

To detect ubiquitin, after lysis and before immunoprecipitation, 1% SDS was added, and the lysates were incubated for 5 min at 90° to dissociate protein–protein interactions. The samples were diluted 10-fold with the same buffer, and the immunoprecipitation assay was performed as described above in this paragraph .

Immunoprecipitates were then washed 5 × 5 min with lysis buffer (40 mM Hepes, pH 7.4, 2 mM EDTA, 0.3% CHAPS, and NaCl 150 mM) and then denatured by adding 1 vol of 4× Laemmli SDS sample buffer with b-mercaptoethanol and incubated at 95° for 10 min.

Proteins were separated on acrylamide gels (Bio-Rad Laboratories) and electroblotted onto nitrocellulose (Protran; Schleicher & Schuell) or polyvinylidene difluoride (EMD Millipore) membranes. Blots were incubated with primary antibodies in 5% nonfat dry milk or 5% BSA in TBS plus 0.1% Tween-20 overnight at 4°C. Detection was achieved using horseradish peroxidase–conjugated secondary antibody (Bio-Rad Laboratories) and visualized with ECL (EMD Millipore).

Of note, in some cases, Western blots were captured using a digital camera (Fluor Chem SP; Alpha Innotec; see Fig. 1, A and E, bottom panels; Fig. 2 C; Fig. 3 E, HA, bottom panel; Fig. 3 F, bottom panels; Fig. 4, B and D; Fig. 5 A, bottom panels; Fig. 6 G; Fig. 7, B–E; and Fig. 8, A–C), whereas in others, they were captured on film (Aurogene). Backgrounds in Western blot images from different

Published December 8, 2016

experimental approaches were then equalized by changing their exposition postacquisition.

RNAi

RNAi was performed using the following RNA oligonucleotide (oligo) duplex from Thermo Fisher Scientific: NEDD4L#1 HSS118597, 5′-CCCAAGACUGCAGAACCCAGCUAUU-3′ (10620318); 5′-AAUAGCUGGGUUCUGCAGUCUUGGG-3′ (10620319); NEDD4L#2 ID: 22855 (3′ UTR), 5′-GGCAUUUAUGUACUACAU-3′; 5′-AUGUAGUACAUAAAGUGCC-3′; ULK1 HSS140824, 5′-GAGAACGUCACCAAGUGCAAGCUGU-3′ (127303D05); 5′-ACAGCUUGCACUUGGUGACGUUCUC-3′ (127303D06); ULK1 (3′UTR) ID: 118261, 5′-CCCAAGCACUUUAUGCAU-3′; 5′-UAUGCAUAAAGUGCUUGGG-3′.

2.5 × 105 cells per well were transfected with 100 pmol siRNA oligos in six-well plates using Lipofectamine 2000 (Thermo Fisher Scientific) following the manufacturer's instructions.

qPCR

Total RNA was isolated by using the RNeasy mini kit (QIAGEN). 2 µg RNA was retrotranscribed using M-MLV enzyme and oligodT (Promega). qPCR was then performed using SYBR Green Mix (Roche) with the LC480 qPCR system (Roche). The following oligos primers were used: *ULK1*, 5′-CAGACAGCCTGATGTGCAGT-3′*;* 5′-CAGGGTGGGGATGGAGAT-3′; *β-ACTIN*: 5′-CCAACCGCGAGAAGATGA-3′; 5′-CCAGAGGCGTACAGGGATAG-3′; *NEDD4L:* 5′-AGCCCAATGGGTCAGAAATAA-3′; 5′-TCTGGACCCTGTTCACAAATC-3′. Melting curve analysis was used to confirm primer specificity. To ensure linearity of the standard curve, reaction efficiencies over the appropriate dynamic range were calculated. Using the ddCt method, we calculated fold-increases in the mRNA expression of the gene of interest normalized to *β-Actin* expression. We then normalized the mRNA levels to the control condition. Reported values are the means of three independent biological replicates with technical triplicates that were averaged for each experiment. Error bars represent SD of the mean.

Immunocytochemistry

Cells were washed in PBS and fixed with 4% paraformaldehyde in PBS for 15 min. After permeabilization with 0.4% Triton X-100 in PBS for 5 min, cells were blocked in 3% horse serum in PBS and incubated overnight at 4°C with primary antibodies. Cells were then washed and incubated for 1 h with labeled anti–mouse (Alexa Fluor 488; Molecular Probes) or anti–rabbit (FITC; Jackson ImmunoResearch Laboratories, Inc.; Alexa Fluor 647 donkey anti–rabbit) secondary antibodies. Images were examined under a confocal laser scanning microscope (FV1000; Olympus) interfaced with 1 × 81 inverted microscope equipped with a 60× (NA 1.35) oil-immersion objective. A 405-nm diode laser was used for the blue channel, a 488-nm argon laser was used for the green channel, and a 543-nm HeNe laser was used for the red channel.

Polysome fractionation

Polysome separation was performed as previously described (Paronetto et al., 2006). In brief, HeLa cells were grown overnight to 60–70% confluence and incubated for the indicated time period (2 and 6 h) in EBSS or control medium. After extensive washing in cold PBS, cells were scraped in lysis buffer (100 mM NaCl, 10 mM $MgCl_2$, 30 mM Tris-HCl, pH 7.5, 1% Triton X-100, 1 mM DTT, 0.5 mM Na_2VO_3, and 25 U/ml RNasin [Promega]) supplemented with protease inhibitor cocktail (Sigma-Aldrich) and lysed by 10-min incubation in ice. Cell lysates were centrifuged for 10 min at 12,000 *g* at 4°C, and the supernatants were collected (cell extracts). 1 mg cell extracts was loaded on a 15–50% (wt/vol) sucrose gradients (10 ml) and sedimented by ultracentrifugation for 2 h at 37,000 rpm in a rotor (SW41; Beckman Coulter). UV-absorption (A_{260}) profiles of polysome gradients were measure by UV detector (UVis-920; GE Healthcare), and each gradient was collected in 10 fractions of 1 ml each. For RT-PCR analysis, 500 µl of fractions 1–5, 6 and 7, and 8–10 were pooled to generate polysomal, 80S, and RNP samples, respectively, and RNA was isolated with RNeasy Mini kit (QIAGEN). Proteins were isolated from the remaining 500 µl of each gradient fraction by adding 50 µl of 72% trichloroacetic acid. Suspensions were mixed, incubated for 15 min in ice, and centrifuged at 12,000 *g* for 10 min at 4°C. Protein pellets were washed with −20°C chilled acetone and resuspended in Laemmli buffer for Western blot analysis.

MTS assay

For the MTS (3-(4,5-dimethylthiazol-2-yl)-5-(3-carboxymethoxyphenyl)-2-(4-sulfophenyl)-2H-tetrazolium) assay, cells were knocked-down for NEDD4L or with control as indicated in the RNAi section. After 48 h of transfection, cells were seeded in 96-well plates (5,000 cells in each well), exposed to full medium or EBSS alone or in combination with Baf A1 for 12 h. During the last hour, MTS was added to the medium. Each combination of cells was analyzed in triplicate wells and analyzed at least three times. The MTS assay was analyzed spectrophotometrically at 490 nm using a 96-well plate reader, as indicated by the supplier (Promega).

Background absorbance were calculated on set of control wells (without cells) containing the same volumes of medium and Baf A1.

MS analysis

Protein elution from ULK1 co-IP was denatured 5 min at 90°C and incubated for 30 min at 56°C with 10 mM DTT for cysteine reduction and 20 min at room temperature with 55 mM iodoacetamide for cysteine alkylation.

Proteins were precipitated by adding five volumes of ethanol 100% (overnight at 4°C) and then centrifuged at 4,000 *g* (40 min at 10°C), resuspended in a buffer containing 2 M urea in 50 mM ammonium bicarbonate, and digested with 0.2 µg trypsin overnight at 37°C.

Tryptic peptides were concentrated with ZipTip mC18 pipette tips (EMD Millipore) and eluted in 80% acetonitrile, 0.1% trifluoroacetic acid. Samples were dried in a vacuum centrifuge and resuspended in 7 µl 2.5%, 0.1% trifluoroacetic acid for the liquid chromatography fractionation and matrix-assisted laser desorption/ionization time-of-flight/time-of-flight (MALDI-TOF/TOF) analysis as described previously (Perdomo et al., 2012; Montaldo et al., 2014). The interpretation of both the MS and MS/MS data was performed with GPS Explorer software (version 3.6; Applied Biosystems) MS peptide fingerprint and MS/MS peptide-sequencing searches were performed against the NCBI nonredundant database using the MASCOT search algorithm. These searches specified trypsin as the digestion enzyme (allowing for one missed trypsin cleavage); carbamidomethylation of cysteine as fixed modification; partial oxidation of methionine; phosphorylation of serine, threonine, and tyrosine; and ubiquitination (glycine–glycine dipeptide) as variable modifications.

Statistical analysis

For all experiments shown, *n* is indicated in the figure legends.

Densitometric analysis was performed using ImageJ software; the mean of the values from different experiments (as indicated) related to the control ratio was arbitrarily defined as 1.00. Each point value represents the mean ± SD or mean ± SEM (as indicated in the figure legends) from three independent experiments unless specified otherwise. Comparison between control and sample in the WB intensity measurement was made from the same Western blot.

Statistical significance was measured using an unpaired Student's *t* test, one-way and two-way analysis of variance (ANOVA) followed by Tukey's post hoc test or Bonferroni's multiple comparison posttest using GraphPad Prism program (version 6) as indicated in the figure legends.

Online supplemental material

Fig. S1 show that ULK1 protein levels are finely regulated upon starvation, but not its interacting proteins, supporting the data shown in Fig. 1. Fig. S2 shows that ULK2 is degraded during autophagy, supporting the data shown in Fig. 3. Fig. S3 shows that NEDD4L is able to bind the kinase-dead ULK1, supporting the data shown in Fig. 4. Fig. S4 shows that the overexpression of ULK1 mutant constructs impairs autophagy dynamics, supporting data shown in Fig. 6. Fig. S5 shows that NEDD4l down-regulation influences cell death, supporting the data shown in Fig. 7. Table S1 shows the identification of ubiquitylation sites of ULK1 protein by MALDI-TOF/TOF analysis.

Acknowledgments

We thank Giuseppe Filomeni for assistance with the preparation of the model in Fig. 9. We thank M. Acuna Villa and M.W. Bennett for editorial and secretarial work.

F. Cecconi's laboratory is supported by grants from the Kræftens Bekæmpelse (KBVU R72-A4408), the Lundbeckfonden (R167-2013-16100), the Novo Nordisk UK Research Foundation (7559), the Associazione Italiana per la Ricerca sul Cancro (IG2013), Fondazione Roma, and in part by Associazione Italiana Sclerosi Multipla (2013), Fondazione Telethon (GGP14202 to F. Cecconi and P. Bonaldo), the Ministero dell'Istruzione dell'Universita e della Ricerca (Fondo per gli Investimenti della Ricerca di Base Accordi di Programma 2011 to F. Cecconi and P. Bonaldo), and the Ministero della Salute (GR2011 to F. Strappazzon and GR-2011-02351643 to S. Campello). This work was also supported by the European Union's Horizon 2020 research and innovation program (Marie Sklodowska-Curie grant agreement 642295 [MEL-PLEX]) F. Cecconi's lab in Copenhagen is part of the newly established Center of Excellence in Autophagy, Recycling and Disease, funded by the Danmarks Grundforskningsfond.

The authors declare no competing financial interests.

Author contributions: F. Nazio designed and performed most experiments with crucial help from M. Carinci (immunoprecipitation), C. Valacca (qPCR), P. Bielli (polysome gradient), F. Strappazzon and S. Campello (confocal analysis), M. Antonioli (ubiquitin assays), and F. Ciccosanti and G.M. Fimia (mass spectrometry and critical reagents). F. Nazio and F. Cecconi wrote the manuscript with the help and suggestions of C. Sette and P. Bonaldo. F. Cecconi conceived the research. All authors discussed the results and commented on the manuscript.

Submitted: 23 May 2016
Revised: 19 September 2016
Accepted: 23 November 2016

References

Alers, S., A.S. Löffler, S. Wesselborg, and B. Stork. 2012. The incredible ULKs. *Cell Commun. Signal.* 10:7. http://dx.doi.org/10.1186/1478-811X-10-7

An, H., D.T. Krist, and A.V. Statsyuk. 2014. Crosstalk between kinases and Nedd4 family ubiquitin ligases. *Mol. Biosyst.* 10:1643–1657. http://dx.doi.org/10.1039/c3mb70572b

Antonioli, M., F. Albiero, F. Nazio, T. Vescovo, A.B. Perdomo, M. Corazzari, C. Marsella, P. Piselli, C. Gretzmeier, J. Dengjel, et al. 2014. AMBRA1 interplay with cullin E3 ubiquitin ligases regulates autophagy dynamics. *Dev. Cell.* 31:734–746. http://dx.doi.org/10.1016/j.devcel.2014.11.013

Behrends, C., M.E. Sowa, S.P. Gygi, and J.W. Harper. 2010. Network organization of the human autophagy system. *Nature.* 466:68–76. http://dx.doi.org/10.1038/nature09204

Bianchini, A., M. Loiarro, P. Bielli, R. Busà, M.P. Paronetto, F. Loreni, R. Geremia, and C. Sette. 2008. Phosphorylation of eIF4E by MNKs supports protein synthesis, cell cycle progression and proliferation in prostate cancer cells. *Carcinogenesis.* 29:2279–2288. http://dx.doi.org/10.1093/carcin/bgn221

Bruce, M.C., V. Kanelis, F. Fouladkou, A. Debonneville, O. Staub, and D. Rotin. 2008. Regulation of Nedd4-2 self-ubiquitination and stability by a PY motif located within its HECT-domain. *Biochem. J.* 415:155–163. http://dx.doi.org/10.1042/BJ20071708

Choi, A.M., S.W. Ryter, and B. Levine. 2013. Autophagy in human health and disease. *N. Engl. J. Med.* 368:651–662. http://dx.doi.org/10.1056/NEJMra1205406

Ding, Y., Y. Zhang, C. Xu, Q.H. Tao, and Y.G. Chen. 2013. HECT domain-containing E3 ubiquitin ligase NEDD4L negatively regulates Wnt signaling by targeting dishevelled for proteasomal degradation. *J. Biol. Chem.* 288:8289–8298. http://dx.doi.org/10.1074/jbc.M112.433185

Dorsey, F.C., K.L. Rose, S. Coenen, S.M. Prater, V. Cavett, J.L. Cleveland, and J. Caldwell-Busby. 2009. Mapping the phosphorylation sites of Ulk1. *J. Proteome Res.* 8:5253–5263. http://dx.doi.org/10.1021/pr900583m

Fotia, A.B., D.I. Cook, and S. Kumar. 2006. The ubiquitin-protein ligases Nedd4 and Nedd4-2 show similar ubiquitin-conjugating enzyme specificities. *Int. J. Biochem. Cell Biol.* 38:472–479. http://dx.doi.org/10.1016/j.biocel.2005.11.006

Füllgrabe, J., M.A. Lynch-Day, N. Heldring, W. Li, R.B. Struijk, Q. Ma, O. Hermanson, M.G. Rosenfeld, D.J. Klionsky, and B. Joseph. 2013. The histone H4 lysine 16 acetyltransferase hMOF regulates the outcome of autophagy. *Nature.* 500:468–471. http://dx.doi.org/10.1038/nature12313

Gao, S., C. Alarcón, G. Sapkota, S. Rahman, P.Y. Chen, N. Goerner, M.J. Macias, H. Erdjument-Bromage, P. Tempst, and J. Massagué. 2009. Ubiquitin ligase Nedd4L targets activated Smad2/3 to limit TGF-beta signaling. *Mol. Cell.* 36:457–468. http://dx.doi.org/10.1016/j.molcel.2009.09.043

Geetha, T., J. Jiang, and M.W. Wooten. 2005. Lysine 63 polyubiquitination of the nerve growth factor receptor TrkA directs internalization and signaling. *Mol. Cell.* 20:301–312. http://dx.doi.org/10.1016/j.molcel.2005.09.014

Georgieva, M.V., Y. de Pablo, D. Sanchis, J.X. Comella, and M. Llovera. 2011. Ubiquitination of TrkA by Nedd4-2 regulates receptor lysosomal targeting and mediates receptor signaling. *J. Neurochem.* 117:479–493. http://dx.doi.org/10.1111/j.1471-4159.2011.07218.x

Goel, P., J.A. Manning, and S. Kumar. 2015. NEDD4-2 (NEDD4L): the ubiquitin ligase for multiple membrane proteins. *Gene.* 557:1–10. http://dx.doi.org/10.1016/j.gene.2014.11.051

Harvey, K.F., A. Dinudom, P. Komwatana, C.N. Jolliffe, M.L. Day, G. Parasivam, D.I. Cook, and S. Kumar. 1999. All three WW domains of murine Nedd4 are involved in the regulation of epithelial sodium channels by intracellular Na+. *J. Biol. Chem.* 274:12525–12530. http://dx.doi.org/10.1074/jbc.274.18.12525

Jiao, H., G.Q. Su, W. Dong, L. Zhang, W. Xie, L.M. Yao, P. Chen, Z.X. Wang, Y.C. Liou, and H. You. 2015. Chaperone-like protein p32 regulates ULK1 stability and autophagy. *Cell Death Differ.* 22:1812–1823. http://dx.doi.org/10.1038/cdd.2015.34

Joo, J.H., F.C. Dorsey, A. Joshi, K.M. Hennessy-Walters, K.L. Rose, K. McCastlain, J. Zhang, R. Iyengar, C.H. Jung, D.F. Suen, et al. 2011. Hsp90-Cdc37 chaperone complex regulates Ulk1- and Atg13-mediated mitophagy. *Mol. Cell.* 43:572–585. http://dx.doi.org/10.1016/j.molcel.2011.06.018

Joo, J.H., B. Wang, E. Frankel, L. Ge, L. Xu, R. Iyengar, X. Li-Harms, C. Wright, T.I. Shaw, T. Lindsten, et al. 2016. The noncanonical role of ULK/ATG1 in ER-to-Golgi trafficking is essential for cellular homeostasis. *Mol. Cell.* 62:491–506. http://dx.doi.org/10.1016/j.molcel.2016.04.020

Jung, C.H., C.B. Jun, S.H. Ro, Y.M. Kim, N.M. Otto, J. Cao, M. Kundu, and D.H. Kim. 2009. ULK-Atg13-FIP200 complexes mediate mTOR signaling to the autophagy machinery. *Mol. Biol. Cell.* 20:1992–2003. http://dx.doi.org/10.1091/mbc.E08-12-1249

Kim, H.C., and J.M. Huibregtse. 2009. Polyubiquitination by HECT E3s and the determinants of chain type specificity. *Mol. Cell. Biol.* 29:3307–3318. http://dx.doi.org/10.1128/MCB.00240-09

Kim, J., M. Kundu, B. Viollet, and K.L. Guan. 2011. AMPK and mTOR regulate autophagy through direct phosphorylation of Ulk1. *Nat. Cell Biol.* 13:132–141. http://dx.doi.org/10.1038/ncb2152

Kuang, E., J. Qi, and Z. Ronai. 2013. Emerging roles of E3 ubiquitin ligases in autophagy. *Trends Biochem. Sci.* 38:453–460. http://dx.doi.org/10.1016/j.tibs.2013.06.008

Lee, I.H., A. Dinudom, A. Sanchez-Perez, S. Kumar, and D.I. Cook. 2007. Akt mediates the effect of insulin on epithelial sodium channels by inhibiting Nedd4-2. *J. Biol. Chem.* 282:29866–29873. http://dx.doi.org/10.1074/jbc.M701923200

Léon, S., and R. Haguenauer-Tsapis. 2009. Ubiquitin ligase adaptors: regulators of ubiquitylation and endocytosis of plasma membrane proteins. *Exp. Cell Res.* 315:1574–1583. http://dx.doi.org/10.1016/j.yexcr.2008.11.014

Li, J., W. Qi, G. Chen, D. Feng, J. Liu, B. Ma, C. Zhou, C. Mu, W. Zhang, Q. Chen, and Y. Zhu. 2015. Mitochondrial outer-membrane E3 ligase MUL1 ubiquitinates ULK1 and regulates selenite-induced mitophagy. *Autophagy.* 11:1216–1229. http://dx.doi.org/10.1080/15548627.2015.1017180

Lin, S.Y., T.Y. Li, Q. Liu, C. Zhang, X. Li, Y. Chen, S.M. Zhang, G. Lian, Q. Liu, K. Ruan, et al. 2012. GSK3-TIP60-ULK1 signaling pathway links growth factor deprivation to autophagy. *Science.* 336:477–481. http://dx.doi.org/10.1126/science.1217032

Liu, C.C., Y.C. Lin, Y.H. Chen, C.M. Chen, L.Y. Pang, H.A. Chen, P.R. Wu, M.Y. Lin, S.T. Jiang, T.F. Tsai, and R.H. Chen. 2016. Cul3-KLHL20 ubiquitin ligase governs the turnover of ULK1 and VPS34 complexes to control autophagy termination. *Mol. Cell.* 61:84–97. http://dx.doi.org/10.1016/j.molcel.2015.11.001

Lu, Z., and T. Hunter. 2009. Degradation of activated protein kinases by ubiquitination. *Annu. Rev. Biochem.* 78:435–475. http://dx.doi.org/10.1146/annurev.biochem.013008.092711

Lu, P.J., X.Z. Zhou, M. Shen, and K.P. Lu. 1999. Function of WW domains as phosphoserine- or phosphothreonine-binding modules. *Science.* 283:1325–1328. http://dx.doi.org/10.1126/science.283.5406.1325

Ma, D., S. Panda, and J.D. Lin. 2011. Temporal orchestration of circadian autophagy rhythm by C/EBPβ. *EMBO J.* 30:4642–4651. http://dx.doi.org/10.1038/emboj.2011.322

Maspero, E., E. Valentini, S. Mari, V. Cecatiello, P. Soffientini, S. Pasqualato, and S. Polo. 2013. Structure of a ubiquitin-loaded HECT ligase reveals the molecular basis for catalytic priming. *Nat. Struct. Mol. Biol.* 20:696–701. http://dx.doi.org/10.1038/nsmb.2566

Mizushima, N. 2010. The role of the Atg1/ULK1 complex in autophagy regulation. *Curr. Opin. Cell Biol.* 22:132–139. http://dx.doi.org/10.1016/j.ceb.2009.12.004

Montaldo, C., C. Mancone, A. Conigliaro, A.M. Cozzolino, V. de Nonno, and M. Tripodi. 2014. SILAC labeling coupled to shotgun proteomics analysis of membrane proteins of liver stem/hepatocyte allows to candidate the inhibition of TGF-beta pathway as causal to differentiation. *Proteome Sci.* 12:15. http://dx.doi.org/10.1186/1477-5956-12-15

Nazio, F., F. Strappazzon, M. Antonioli, P. Bielli, V. Cianfanelli, M. Bordi, C. Gretzmeier, J. Dengjel, M. Piacentini, G.M. Fimia, and F. Cecconi. 2013. mTOR inhibits autophagy by controlling ULK1 ubiquitylation, self-association and function through AMBRA1 and TRAF6. *Nat. Cell Biol.* 15:406–416. http://dx.doi.org/10.1038/ncb2708

Noda, N.N., and Y. Fujioka. 2015. Atg1 family kinases in autophagy initiation. *Cell. Mol. Life Sci.* 72:3083–3096. http://dx.doi.org/10.1007/s00018-015-1917-z

Orvedahl, A., R. Sumpter Jr., G. Xiao, A. Ng, Z. Zou, Y. Tang, M. Narimatsu, C. Gilpin, Q. Sun, M. Roth, et al. 2011. Image-based genome-wide siRNA screen identifies selective autophagy factors. *Nature.* 480:113–117. http://dx.doi.org/10.1038/nature10546

Paronetto, M.P., F. Zalfa, F. Botti, R. Geremia, C. Bagni, and C. Sette. 2006. The nuclear RNA-binding protein Sam68 translocates to the cytoplasm and associates with the polysomes in mouse spermatocytes. *Mol. Biol. Cell.* 17:14–24. http://dx.doi.org/10.1091/mbc.E05-06-0548

Perdomo, A.B., F. Ciccosanti, O.L. Iacono, C. Angeletti, M. Corazzari, N. Daniele, A. Testa, R. Pisa, G. Ippolito, G. Antonucci, et al. 2012. Liver protein profiling in chronic hepatitis C: identification of potential predictive markers for interferon therapy outcome. *J. Proteome Res.* 11:717–727. http://dx.doi.org/10.1021/pr2006445

Petherick, K.J., O.J.L. Conway, C. Mpamhanga, S.A. Osborne, A. Kamal, B. Saxty, and I.G. Ganley. 2015. Pharmacological inhibition of ULK1 kinase blocks mammalian target of rapamycin (mTOR)-dependent autophagy. *J. Biol. Chem.* 290:11376–11383. http://dx.doi.org/10.1074/jbc.C114.627778

Platta, H.W., H. Abrahamsen, S.B. Thoresen, and H. Stenmark. 2012. Nedd4-dependent lysine-11-linked polyubiquitination of the tumour suppressor Beclin 1. *Biochem. J.* 441:399–406. http://dx.doi.org/10.1042/BJ20111424

Procaccini, C., V. De Rosa, M. Galgani, L. Abanni, G. Calì, A. Porcellini, F. Carbone, S. Fontana, T.L. Horvath, A. La Cava, and G. Matarese. 2010. An oscillatory switch in mTOR kinase activity sets regulatory T cell responsiveness. *Immunity.* 33:929–941. http://dx.doi.org/10.1016/j.immuni.2010.11.024

Sahani, M.H., E. Itakura, and N. Mizushima. 2014. Expression of the autophagy substrate SQSTM1/p62 is restored during prolonged starvation depending on transcriptional upregulation and autophagy-derived amino acids. *Autophagy.* 10:431–441. http://dx.doi.org/10.4161/auto.27344

Schiaffino, S., C. Mammucari, and M. Sandri. 2008. The role of autophagy in neonatal tissues: just a response to amino acid starvation? *Autophagy.* 4:727–730. http://dx.doi.org/10.4161/auto.6143

Shearwin-Whyatt, L., H.E. Dalton, N. Foot, and S. Kumar. 2006. Regulation of functional diversity within the Nedd4 family by accessory and adaptor proteins. *BioEssays*. 28:617–628. http://dx.doi.org/10.1002/bies.20422

Wirth, M., J. Joachim, and S.A. Tooze. 2013. Autophagosome formation--the role of ULK1 and Beclin1-PI3KC3 complexes in setting the stage. *Semin. Cancer Biol.* 23:301–309. http://dx.doi.org/10.1016/j.semcancer.2013.05.007

Wong, P.M., Y. Feng, J. Wang, R. Shi, and X. Jiang. 2015. Regulation of autophagy by coordinated action of mTORC1 and protein phosphatase 2A. *Nat. Commun.* 6:8048. http://dx.doi.org/10.1038/ncomms9048

Xia, P., S. Wang, G. Huang, Y. Du, P. Zhu, M. Li, and Z. Fan. 2014. RNF2 is recruited by WASH to ubiquitinate AMBRA1 leading to downregulation of autophagy. *Cell Res.* 24:943–958. http://dx.doi.org/10.1038/cr.2014.85

Yang, B., and S. Kumar. 2010. Nedd4 and Nedd4-2: closely related ubiquitin-protein ligases with distinct physiological functions. *Cell Death Differ.* 17:68–77. http://dx.doi.org/10.1038/cdd.2009.84

Yu, L., C.K. McPhee, L. Zheng, G.A. Mardones, Y. Rong, J. Peng, N. Mi, Y. Zhao, Z. Liu, F. Wan, et al. 2010. Termination of autophagy and reformation of lysosomes regulated by mTOR. *Nature.* 465:942–946. http://dx.doi.org/10.1038/nature09076

Zhou, X., J.R. Babu, S. da Silva, Q. Shu, I.A. Graef, T. Oliver, T. Tomoda, T. Tani, M.W. Wooten, and F. Wang. 2007. Unc-51-like kinase 1/2-mediated endocytic processes regulate filopodia extension and branching of sensory axons. *Proc. Natl. Acad. Sci. USA.* 104:5842–5847. http://dx.doi.org/10.1073/pnas.0701402104

Nazio et al., https://doi.org/10.1083/jcb.201605089

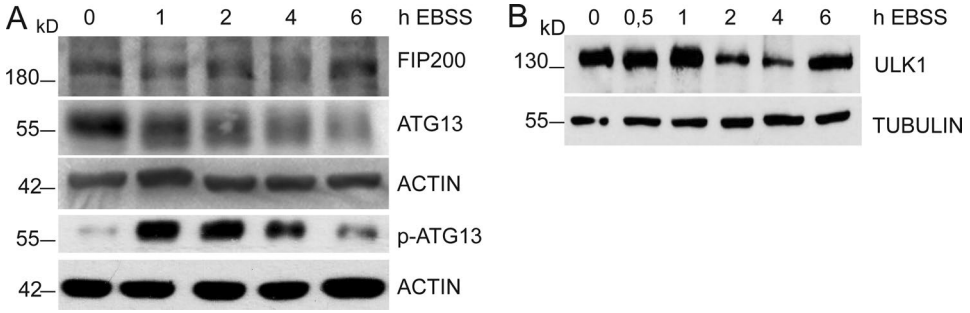

Figure S1. **The expression profile of ULK1 and its interactors during starvation.** (A) HeLa cells were treated with EBSS for the indicated time points, and the levels of FIP200, ATG13, p-ATG13, and ACTIN were detected by WB. (B) HEK 293 cells were treated with EBSS for the indicated time points, and the levels of ULK1 and TUBULIN were detected by WB.

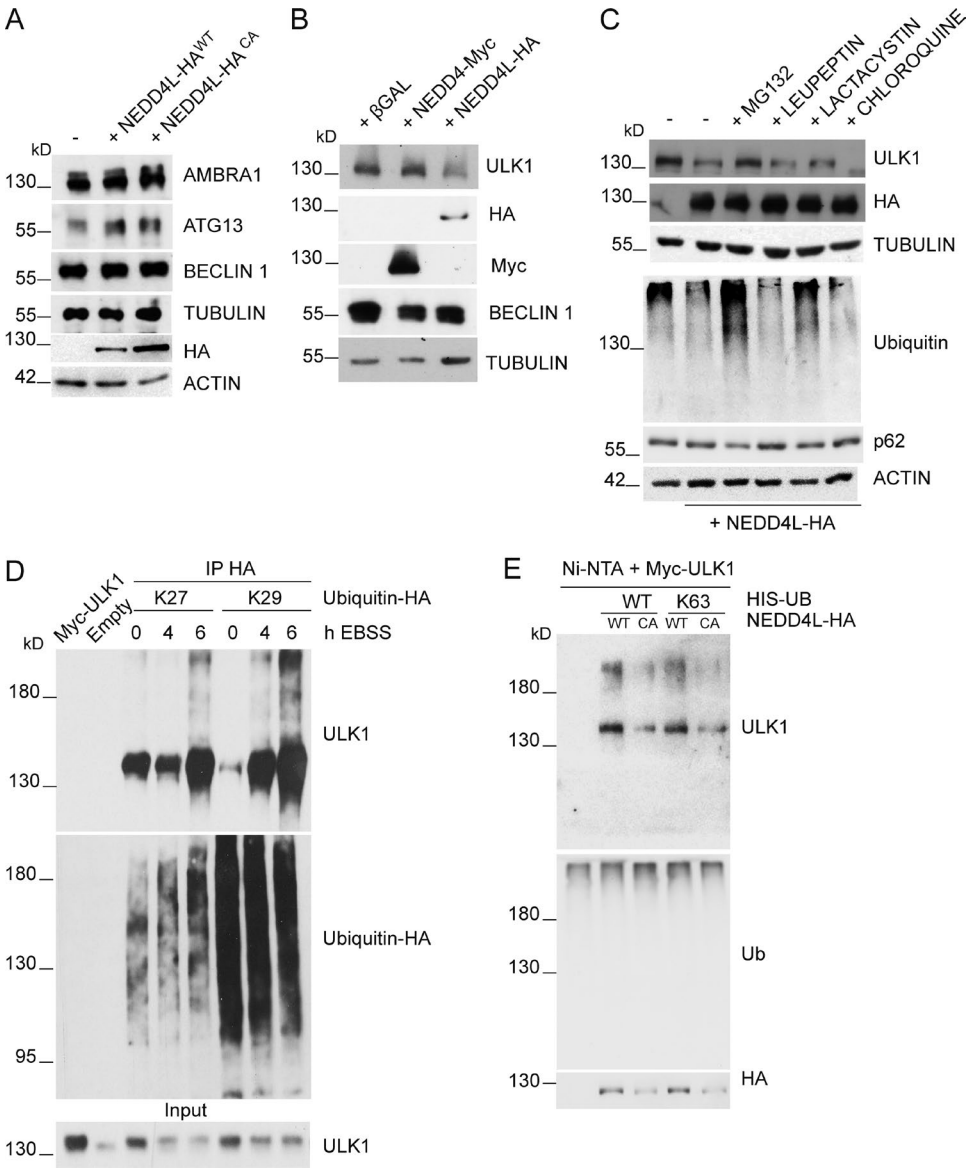

Figure S2. **Analysis of ULK1 degradation processes.** (A) HeLa cells were transfected with NEDD4L^{WT} or NEDD4L^{CA} HA-tagged cDNA, and the levels of AMBRA1, ATG13, BECLIN 1, NEDD4L, ACTIN, and TUBULIN were detected by WB. (B) HeLa cells were transfected with NEDD4L-HA or NEDD4-Myc; the levels of ULK1, NEDD4-Myc, NEDD4L-HA, BECLIN 1, and TUBULIN were detected by WB. (C) HeLa cells were transfected with NEDD4L-HA in the presence of two different proteasomal inhibitors (MG132 and lactacystin) or two different autophagy inhibitors (Clq and leupeptin); the levels of ULK1, NEDD4L, TUB ULIN, p62, ubiquitin, and ACTIN were detected by WB. (D) HeLa cells were cotransfected with Myc-ULK1 and HA-tag specific ubiquitin constructs (K29 and K27) and treated with EBSS for the indicated time points. Protein extracts were immunoprecipitated in denaturing conditions using an anti-HA antibody; ubiquitin and ULK1 were analyzed by WB. (E) HeLa cells were cotransfected with a vector encoding two 6xHIS-tag specific ubiquitin constructs (WT and K63) and Myc-ULK1 in combination or not with NEDD4L^{WT}-HA or NEDD4L^{CA}-HA tagged proteins as a negative control. Protein extracts were prepared as in Fig. 4 F, and the amount of ubiquitylated ULK1 copurified with 6xHIS-ubiquitin was evaluated by WB using anti-ULK1 antibody.

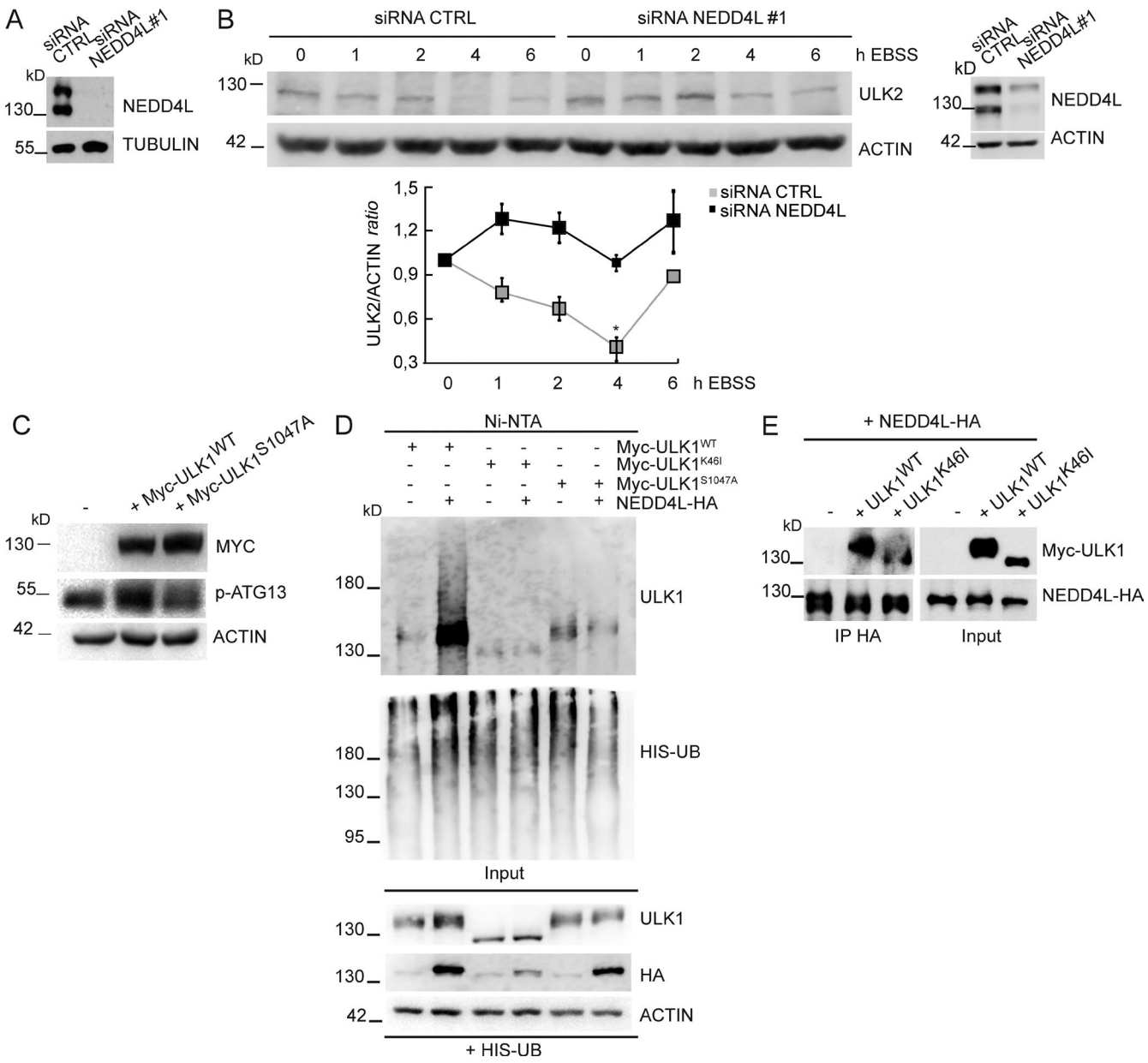

Figure S3. **Analysis of NEDD4L on ULK molecular species.** (A) WB related to Fig. 4 C. NEDD4L expression was down-regulated in HeLa cells using specific RNAi oligos (siRNA NEDD4L#1) or unrelated oligos as negative control (siRNA CTRL). The levels of NEDD4L and TUBULIN were detected by WB. (B) NEDD4L expression was down-regulated as in (A) and autophagy was induced by starving cells for the indicated time periods. Levels of ULK2 and ACTIN were detected by WB. Densitometric analysis of ULK2 over ACTIN is also shown (below the graph). Data are expressed as the mean ± SEM (n = 3) and were analyzed by two-way ANOVA followed by Bonferroni's multiple comparison post test. *, $P < 0.05$. (C) HeLa cells were cotransfected with cDNAs coding for Myc-tagged ULK1^{WT} or ULK1^{S1047A}. The levels of ULK1, p-ATG13, and ACTIN were detected by WB. (D) HeLa cells were cotransfected with a vector encoding a 6xHIS-tag ubiquitin and cDNAs coding for Myc-tagged ULK1^{WT} or ULK1^{K46I} or ULK1^{S1047A} in the presence or not of NEDD4L^{WT}-HA and in the presence of MG132. Protein extracts were prepared in a denaturing urea buffer and subjected to Ni-NTA purification. The amount of ubiquitylated ULK1 copurified with 6xHIS-ubiquitin was evaluated by WB using anti-ULK1 antibody. (E) HeLa cells were cotransfected with cDNAs coding for Myc-tagged ULK1^{WT} or ULK1^{K46I} together with NEDD4L^{WT}-HA. Protein extracts were immunoprecipitated using an anti-HA antibody and analyzed by WB using anti-Myc and anti-HA antibodies.

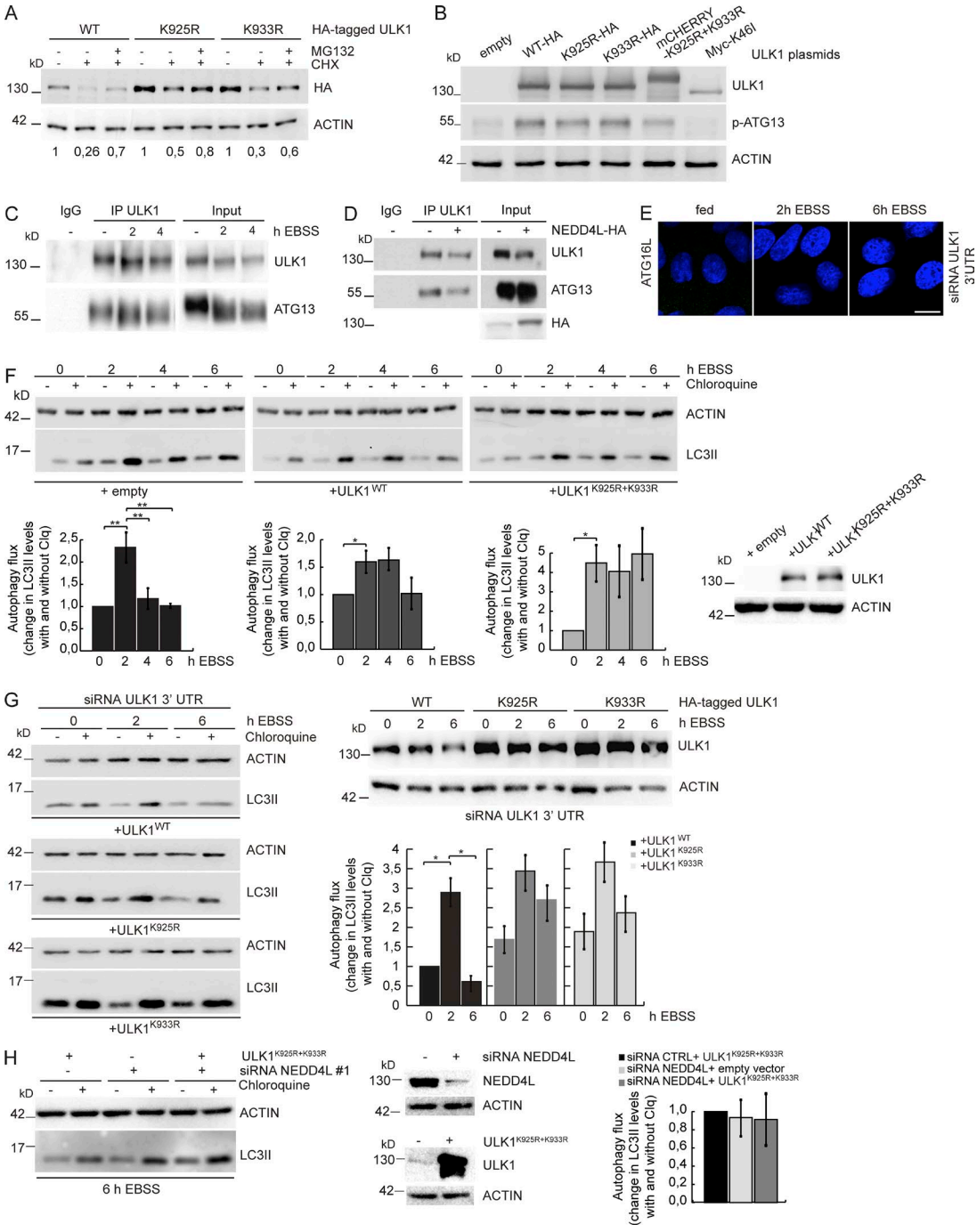

Figure S4. **Study of ULK1 degradation mutants during autophagy.** (A) HeLa cells were transfected with ULK1^{WT}, ULK1^{K925R}, and ULK1^{K933R} HA-tagged proteins and treated with CHX or MG132. The levels of ULK1 and ACTIN were detected by WB. Densitometric analysis of ULK1 over ACTIN is also shown. (B) HeLa cells were transfected with ULK1^{WT}, ULK1^{K925R}, and ULK1^{K933R} HA-tagged proteins, mCherry-ULK1 $^{K925R+K933R}$, and Myc-ULK1 ^{K46I}, respectively. The levels of ULK1, p-ATG13, and ACTIN were detected by WB. (C) HeLa cells were treated with EBSS for the indicated time points, and protein extracts were immunoprecipitated using anti-ULK1 antibody or with IgG as a negative control. ATG13 and ULK1 were analyzed by WB. (D) HeLa cells were transfected with empty vector or NEDD4L^{WT} HA-tagged cDNA; protein extracts were immunoprecipitated using anti-ULK1 antibody or with IgG as a negative control and analyzed by WB using anti-ATG13 and anti-ULK1 antibodies. (E) Representative images for the negative control related to Fig. 6 G. Bar, 20 µm. (F) HeLa cells were transfected with empty, ULK1^{WT}, or ULK1$^{K925R+K933R}$ mCherry-tagged plasmids, respectively, and autophagy was induced with EBSS for the indicated time points in the presence or absence of Clq. Densitometric analysis of LC3II+Clq-LC3II control over ACTIN band is also shown (below the graph). Data are expressed as the mean ± SEM (n = 3) and were analyzed by one-way ANOVA followed by Tukey post hoc test. *, P < 0.05; **, P < 0.01. (G) Endogenous ULK1 was silenced by RNAi, and then HeLa cells were transfected with ULK1^{WT}, ULK1^{K925R}, and ULK1^{K933R} HA-tagged proteins and autophagy was induced with EBSS for the indicated time points in the presence or absence of Clq. The levels of LC3II and ACTIN were detected by WB. Densitometric analysis of LC3II+Clq/LC3II control over ACTIN band is also shown (below the graph). Data are expressed as the mean ± SEM (n = 3) and were analyzed by one-way ANOVA followed by Tukey post hoc test. *, P < 0.05. (H) NEDD4L was down-regulated by RNAi, and then HeLa cells were transfected with empty vector or mCherry-ULK1$^{K925R+K933R}$, respectively. Autophagy was induced for 6 h. The levels of LC3 and ACTIN were detected by WB. Densitometric analysis of LC3II+Clq/LC3II control over ACTIN band is also shown. Data are expressed as the mean ± SEM (n = 3) and were analyzed by one-way ANOVA followed by Tukey post hoc test.

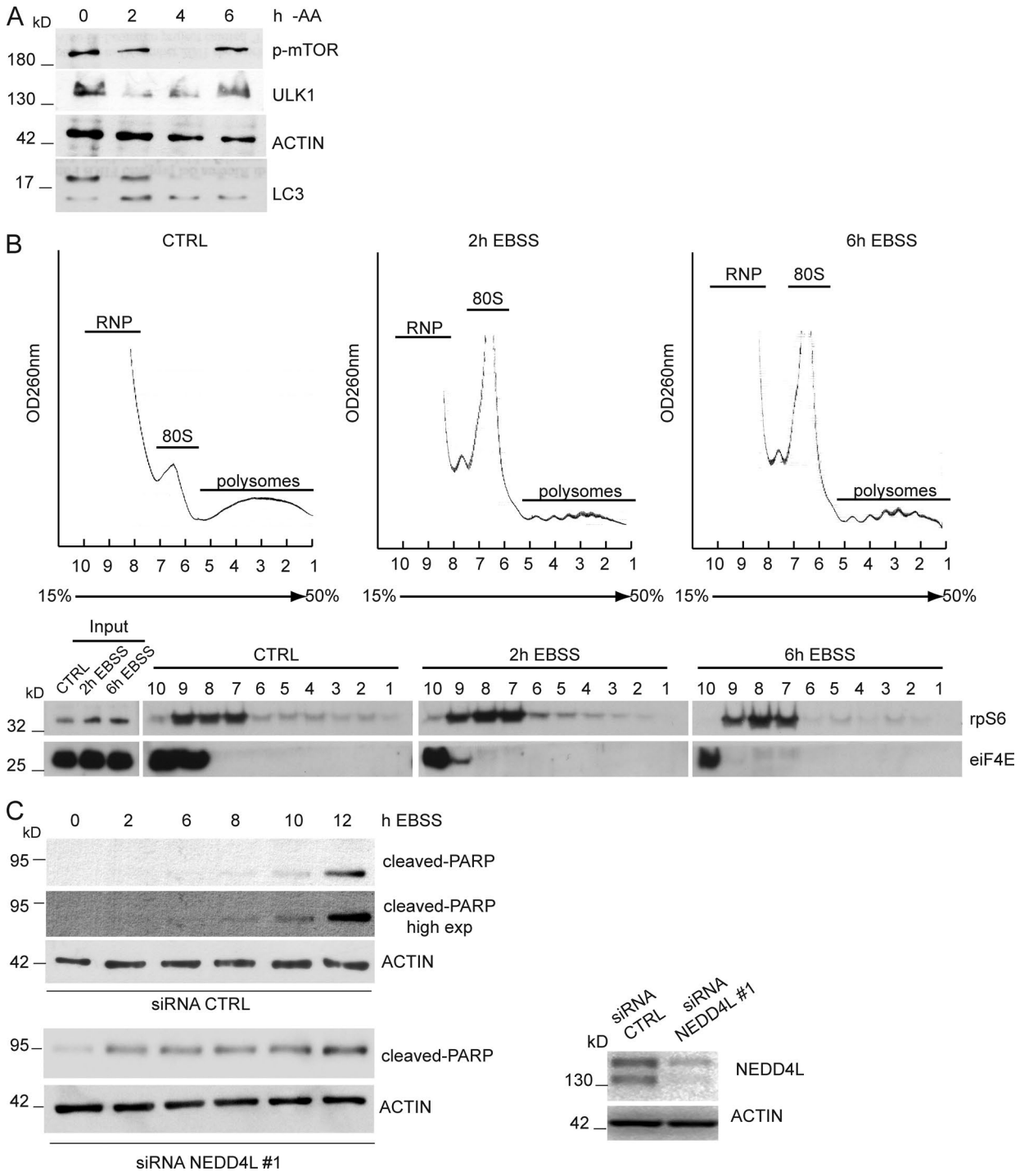

Figure S5. **Analysis of mTOR-mediated protein synthesis and cell death upon prolonged starvation.** (A) HeLa cells were treated with a medium without amino acids for the indicated time points, and the levels of p-mTOR, ULK1, LC3, and ACTIN were detected by WB. (B) Representative absorption profiles (A_{260}) of sucrose gradient fractionation of control (CTRL) and EBSS-starved (2 h EBSS and 6 h EBSS) HeLa cell extracts (top). Gradients were collected in 10 fractions, and Western blot analyses of each fraction indicated the distribution of the ribosomal S6 protein (rpS6) and of initiation factor eIF4E (bottom). (C) NEDD4L expression was down-regulated in HeLa cells using specific RNAi oligos (siRNA NEDD4L#1) and treated with EBSS for the indicated time points. The levels of cleaved-PARP, NEDD4L, and ACTIN were detected by WB.

Provided online is Table S1, showing the identification of ubiquitination sites of ULK1 protein by MALDI-TOF/TOF analysis.